NAVAL POSTGRADUATE SCHOOL

MONTEREY, CALIFORNIA

THESIS

AN INVESTIGATION OF SURFACE CURRENT PATTERNS RELATED TO UPWELLING IN MONTEREY BAY, USING HIGH FREQUENCY RADAR

by

Andres Enriquez

June 2004

Thesis Advisor:	Jeffrey Paduan
Second Reader:	Mary Batteen

Approved for public release; distribution is unlimited

THIS PAGE INTENTIONALLY LEFT BLANK

REPORT DOCUMENTATION PAGE			Form Approved OMB No. 0704-0188
Public reporting burden for this collection of information is estimated to average 1 hour per response, including the time for reviewing instruction, searching existing data sources, gathering and maintaining the data needed, and completing and reviewing the collection of information. Send comments regarding this burden estimate or any other aspect of this collection of information, including suggestions for reducing this burden, to Washington headquarters Services, Directorate for Information Operations and Reports, 1215 Jefferson Davis Highway, Suite 1204, Arlington, VA 22202-4302, and to the Office of Management and Budget, Paperwork Reduction Project (0704-0188) Washington DC 20503.			
1. AGENCY USE ONLY *(Leave blank)*	**2. REPORT DATE** Month Year	**3. REPORT TYPE AND DATES COVERED** Master's Thesis	
4. TITLE AND SUBTITLE: An Investigation of Surface Current Patterns Related to Upwelling in Monterey Bay using High Frequency Radar		**5. FUNDING NUMBERS**	
6. AUTHOR(S) **Enriquez, Andres E.**			
7. PERFORMING ORGANIZATION NAME(S) AND ADDRESS(ES) Naval Postgraduate School Monterey, CA 93943-5000		**8. PERFORMING ORGANIZATION REPORT NUMBER**	
9. SPONSORING /MONITORING AGENCY NAME(S) AND ADDRESS(ES) N/A		**10. SPONSORING/MONITORING AGENCY REPORT NUMBER**	
11. SUPPLEMENTARY NOTES The views expressed in this thesis are those of the author and do not reflect the official policy or position of the Department of Defense or the U.S. Government.			
12a. DISTRIBUTION / AVAILABILITY STATEMENT Approved for public release; distribution is unlimited		**12b. DISTRIBUTION CODE**	

13. ABSTRACT (maximum 200 words)

High Frequency (HF) radar backscatter instruments are under development and testing in the marine science and defense science communities for their abilities to remotely sense surface parameters in the coastal ocean over large areas. In the Navy context, the systems provide real-time mapping of ocean surface currents and waves critical to characterization and forecasting of the battlespace environment. In this study, HF radar, aircraft and satellite information were used to investigate and describe surface current in Monterey Bay, California, for a period of ten months, from June 01st, 2003 to March 31st, 2004. A network of five CODAR-type HF radar instruments measured hourly surface currents over the bay. The measurements were averaged over one-hour intervals and total surface velocities were mapped on a grid in the Monterey Bay. From the M1 Buoy located in the middle of the bay, an uninterrupted time series of wind intensity and direction was obtained for the whole period. Major upwelling events were observed during the period of June 14 to June 27, July 4 to July 19, August 8 to August 18 and other upwelling events were observed until late October. These periods of upwelling favorable winds are common during summer with durations of 10 to 20 days. Often they are interrupted by periods of relaxation state of just a few days as the winds veer to the northwest or northeast. Cyclonic circulation cells are developed on shore during upwelling conditions and an anticyclonic circulation in the middle of the bay is observed when the wind shifts to the southwest producing a strong flow out of the bay close to the coastline off Point Piños. Downwelling conditions are much common less than upwelling, with occurrences during winter and early fall storms with events lasting between two to five days. When the wind blows to the northeast with an intensity of 4 m/s or more for more than 12 hours, a well developed anticyclonic gyre forms in the middle of the bay. This is associated with a strong current, 35 to 40 cm/s, which flushes out in the southern part of the bay close to the coast off Point Piños. This flow reverses when the winds veer to the southwest and enter into the Bay with less intensity.

14. SUBJECT TERMS High Frequency Radar, Upwelling, Monterey Bay Circulation, Surface-Current Maps, Relaxation Periods.			**15. NUMBER OF PAGES** 101
			16. PRICE CODE
17. SECURITY CLASSIFICATION OF REPORT Unclassified	**18. SECURITY CLASSIFICATION OF THIS PAGE** Unclassified	**19. SECURITY CLASSIFICATION OF ABSTRACT** Unclassified	**20. LIMITATION OF ABSTRACT** UL

NSN 7540-01-280-5500

Standard Form 298 (Rev. 2-89)
Prescribed by ANSI Std. 239-18

THIS PAGE INTENTIONALLY LEFT BLANK

Approved for public release; distribution is unlimited

AN INVESTIGATION OF SURFACE CURRENT PATTERNS RELATED TO UPWELLING IN MONTEREY BAY, USING HIGH FREQUENCY RADAR

Andres E. Enriquez
First Lieutenant, Chilean Navy
B.S. Chilean Naval Polytechnic Academy, 1997

Submitted in partial fulfillment of the
requirements for the degree of

MASTER OF SCIENCE IN PHYSICAL OCEANOGRAPHY

from the

NAVAL POSTGRADUATE SCHOOL
June 2004

Author: Andres E. Enriquez

Approved by: Jeffrey Paduan
Thesis Advisor

Mary Batteen
Second Reader

Mary Batteen
Chairman, Department of Oceanography

THIS PAGE INTENTIONALLY LEFT BLANK

ABSTRACT

High Frequency (HF) radar backscatter instruments are under development and testing in the marine science and defense science communities for their abilities to remotely sense surface parameters in the coastal ocean over large areas. In the Navy context, the systems provide real-time mapping of ocean surface currents and waves critical to characterization and forecasting of the battlespace environment. In this study, HF radar, aircraft and satellite information were used to investigate and describe surface current in Monterey Bay, California, for a period of ten months, from June 01st, 2003 to March 31st, 2004. A network of five CODAR-type HF radar instruments measured hourly surface currents over the bay. The measurements were averaged over one-hour intervals and total surface velocities were mapped on a grid in the Monterey Bay. From the M1 Buoy located in the middle of the bay, an uninterrupted time series of wind intensity and direction was obtained for the whole period. Major upwelling events were observed during the period of June 14 to June 27, July 4 to July 19, August 8 to August 18 and other upwelling events were observed until late October. These periods of upwelling favorable winds are common during summer with durations of 10 to 20 days. Often they are interrupted by periods of relaxation state of just a few days as the winds veer to the northwest or northeast. Cyclonic circulation cells are developed on shore during upwelling conditions and an anticyclonic circulation in the middle of the bay is observed when the wind shifts to the southwest producing a strong flow out of the bay close to the coastline off Point Piños. Downwelling conditions are much common less than upwelling, with occurrences during winter and early fall storms with events lasting between two to five days. When the wind blows to the northeast with an intensity of 4 m/s or more for more than 12 hours, a well developed anticyclonic gyre forms in the middle of the bay. This is associated with a strong current, 35 to 40 cm/s, which flushes out in the southern part of the bay close to the coast off Point Piños. This flow reverses when the winds veer to the southwest and enter into the Bay with less intensity.

THIS PAGE INTENTIONALLY LEFT BLANK

TABLE OF CONTENTS

THIS PAGE INTENTIONALLY LEFT BLANK

LIST OF FIGURES

LIST OF TABLES

THIS PAGE INTENTIONALLY LEFT BLANK

ACKNOWLEDGMENTS

The work in this thesis involved many to whom I owe much for their assistance and support.

I would like to thank my advisor, Jeffrey Paduan, for letting me work with him and for his constant support and patience during this research. I would like to thank to Fred Bahr for his constant assistance with the data processing and for his goodwill every time I asked him for help.

I would like to specially thank Mike Cook who gave me constant support and invaluable assistance in computing programming.

I would like to thank Professor Mary Batteen for her support and advice during the time I spent in the Department of Oceanography of the Naval Postgraduate School.

I also would like to thank MBARI for the use of the M1 mooring data and to the PISCO program for the use of the Hopkins Marine Station and Terrace Point ADCP data.

Most importantly I would like to thank my wife, Maria Teresa, for her unconditional support, patience and encouragement not only during the thesis period but during the two years I spent at the Naval Postgraduate School.

THIS PAGE INTENTIONALLY LEFT BLANK

I. INTRODUCTION

A. BACKGROUND

1. Large-Scale Circulation

The dynamics of the coast of California is particularly difficult because of the large-scale, sub-tropical oceanic circulation in the North Pacific Ocean, which is dominated by the clockwise ocean gyre driven by the anticyclonic atmospheric. Several circulations of counter flow are present in the area. The Inshore Countercurrent, (IC), Davison Current (DC) Southern California Countercurrent (SSC), Southern California Eddy (SCE) and California Undercurrent (CU) form finally the California Current System (CCS). The CCS is an eastern boundary current system which extends from the Strait of Juan de Fuca southward to the tip of Baja California Peninsula. It is an offshore (800-900Km), near-surface (0~300 m) equatorialward flow with low salinity, relatively low temperature and with speeds of about 10 cm s^{-1}. Seasonal variations in alongshore wind stress, coastline irregularities, bottom topography, temperature and salinity variation have been shown to be the mechanism responsible for the observed large-scale structure within the CCS (Hickey, 1998).

Along the coast north of Pt. Reyes, the alongshore wind stress is persistently from the north and does not reverse direction, while along the Mendocino coast and further north the direction of the wind stress changes seasonally (Strub et al. 1987). During late fall and winter, the winds become more variable as storms periodically reverse the wind direction. Maximum seasonal wind stress at 35^0 N occurs from May to June whereas at 39^0 N the maximum wind stress occurs in July. The seasonal variation in wind patterns has several effects: when winds are strong from the northwest between March and September along the central California coast, the wind-driven (Ekman) transport of the waters between the surface and about 50 m has an offshore component. The sea surface is lowest along the coast and tilts upward by about 20 cm across the width of the California Current (1000 km). Deeper upwelled waters, which flow shoreward and upward beneath the Ekman layer, replace surface waters

moved seaward. Upwelling speeds may reach 1 m/day or greater (Breaker and Mooers 1986), under favorable wind conditions and from depths as great as 200 m (Smith 1968).

Within the coastal regime, the sea surface flow undergoes a seasonal reversal during late fall and winter. The direction is primarily poleward while the equatorward flow dominates during the spring and summer. The equatorward flow is coupled with intensification of northwesterly winds that generally parallel the central California coastline. This pressure gradient begins to form and to strengthen in the spring. The sudden strengthening of the northwesterly winds, usually from March to May, may result in the “spring transition” in which upwelling commences and local sea surface temperature fall by as much as 5^0 C within a few days. Surface waters are advected offshore and the equatorward geostrophic flow is established after baroclinic adjustment. During late fall, the North Pacific High weakens and migrates southward and the thermal low disappears. The surface flow reverses to poleward and can be regarded as the surface signature of the California Undercurrent (CU), although some investigators refer to this poleward current as the Davison Current, mentioned previously.

Satellite imagery, field studies using Langarian drifters, and recent numerical modeling suggest the existence of numerous large-scale (50-300 km), and long-lived (20-40 days) jets and meanders in the region offshore of the northern California Shelf (Hickey, 1998).

2. Monterey Bay Circulation

Monterey Bay is one of several large bays located on the west coast of the United States about 100 km south of San Francisco. The coastline forms a semi-enclosed bay with both a shallow narrow shelf and the Monterey Canyon, with depths exceeding 2000 m. The regional circulation in the Monterey Bay area is tightly coupled to the CCS and highly correlated to the coastal upwelling. Understanding the variability of the surface transport of Monterey Bay and at the

same time identifying the transport pathway is important for addressing both practical problems as well as fundamental research questions regarding the coastal ocean.

The surface current around the bay has strong variability that is well separated in terms of timescales. It seems that for longer timescales, that is, for periods of weeks and even months, mesoscale patterns evolve with major wind reversals and the proximity of mesoscale eddies (Paduan and Rosenfeld 1996). At shorter timescales, current fluctuations are dominated by semidiurnal tidal forcing and diurnal wind (seabreeze) forcing (Foster 1993; Petruncio 1993). Previous studies (Ramp et al.1997; Collins et al.1996) have shown that currents over the slope of Central California are dominated by long-period fluctuations. These fluctuations have generally been associated with the offshore eddy and meander field.

Three different seasonal faces were described by Skogsberg (1936) during an extensive oceanography study of Monterey Bay between 1929 and 1933. The first of these seasonal faces is called the “upwelling period” and is driven by upwelling-favorable winds that extend from mid-February until August-September. Along the Central California coast, winds from the northwest associated with the subtropical high pressure cells produce coastal upwelling, which in turn influences the coastal circulation and thermal structure strongly. In the Monterey area, coastal upwelling usually occurs between March and October (Breaker and Broenkow 1994). Upwelling centers in the Monterey area are located near Point Año Nuevo and Point Sur (Paduan and Rosenfeld 1996).

The “oceanic period” extends from late summer to early fall. Skogsberg (1936) attributed this period to the onshore movement of oceanic waters associated with the CC. During this period, the North Pacific High weakens, wind stress relaxes, and the cool upwelled waters begin to sink and are replaced by warmer surface water from offshore. Coastal sea surface temperatures rise to their highest seasonal values and strong vertical temperatures gradients form (Breaker et al. 1994). Rosenfeld et al. (1994) named this period as a “relaxation

state” in which the Monterey area is characterized by rapid onshore advection of warm oceanic water combined with surface warming.

Finally, the “Davison Current Period” goes from December to early February, coinciding with the local occurrence of the northward DC. Strong southerly winds generate onshore Ekman transport, resulting in a general rise in the sea level, which in turn, causes downwelling and offshore cross-shelf flow below the Ekman layer.

Rosenfeld et al. (1994) also focused on the Monterey Bay, and observed the development of a warm, fresh anticyclonic eddy at the entrance or just to the south of the bay, when upwelling immediately followed a relaxation event. Satellite observations suggest that a meander or a warm-core eddy, 50 to 100 Km in diameter, may be present occasionally just west of Monterey Bay (Breaker, et al. 1994).

3. Wind Pattern

The wind along the west coast of the United States is governed primarily by the location of the Eastern Pacific Subtropical High, which dominates the large-scale wind field during summer but reverses direction north of San Francisco during the winter. Equatorward wind stress occurs during the spring in southern California and in the northern area during the summer and minimum equatorward wind stress occurs during late fall. Wind intensity is proportional to the barometric pressure difference between the North Pacific High and the thermal low pressure centered in southern Nevada and California.

A ten-year time series of the Monterey Bay seasonal, interannual and long-term wind fluctuations were collected between 1989 and 1998 by the Monterey Bay Aquarium Research Institute MBARI, including data from the 1992 to 1993 and 1997 to 1998 El Niño events. The data were collected from ship surveys, and supplemented by moored observations of current and wind, as well as satellite observations of temperature and ocean color providing spatial coverage. The results indicated that daily winds offshore of Monterey Bay are

predominantly from the northwest at 5 to 10 m/s, with interruptions primarily in winter (MBARI-BOG: 10 year study from Monterey Bay, Seasonal Patterns). Alongshore-daily winds stress is thus predominantly equatorward with reversals in winter. The average year of alongshore wind stress shows intermittent positive (poleward) stresses from December to March, minimum negative (equatorward) stress in April and June, and moderate negative stresses from July to November.

4. Upwelling

In general, coastal upwelling occurs along eastern ocean margins when equatorward winds act in combination with the Coriolis force to move surface waters offshore, drawing deeper water to the surface. This “upwelled” water occurs as a cool band along the coast typically tens of kilometers broad, separated from warmer waters offshore. The coastal ocean off western North America has received considerable oceanographic research because of the fisheries supported by the upwelling processes and because of its proximity to large human populations. The oceanography of this region is strongly influenced by the process of coastal upwelling. In general terms, in the northeast Pacific Ocean coastal upwelling occurs seasonally.

In the Monterey Bay, which is the site of the present study, the available information on currents and upwelling indicates a complex and sometimes contradictory picture of the structure in this region. In 1989, MBARI began an intensive study of the coastal upwelling system of central California (Chavez 1997) incorporating biweekly to monthly ship expeditions together with continuous observations from moored platforms. In general terms, the Monterey Bay regional circulation can be described in two distinct hydrographic states: Upwelling state (1-3 weeks) and Relaxation state (3-6 days). These two periods are related to the prevailing wind patterns. In summer, which is the upwelling period, the typical circulation in the bay consists of an upwelling front originating from Pt. Año Nuevo, a cyclonic circulation inshore of the front and another upwelling region off Pt. Sur. When the wind relaxes, the upwelling reduces and the offshore eddy circulation, which is assumed to be part of the CC meandering

flow system, flows into the bay and interacts with the flow over the shelf. Rosenfeld et al. (1994) investigated the upwelling center off Point Año Nuevo north of the bay. They suggested that the surface waters enter the Monterey Bay principally from the north, while Broenkow and Smethie (1978) suggest the flow into the bay is often from the south. Recently AVHRR satellite images often reveal a tongue of cool water extending across the mouth of the bay. Other AVHRR images in April 1993 revealed two symmetrical, apparently anticyclonic eddies southwest of San Francisco and Monterey Bay with cool coastal waters near Point Año Nuevo and Point Sur.

When upwelling ceases, sometimes abruptly, at the end of summer (typically August, September) the sea level along the coast and inside the Monterey Bay rises and the California Current slows. Sea surface temperatures along the coast may rise markedly. Later in the year (typically November) when winter storms bring occasional strong northward winds, Ekman transport is shoreward, and in places the surface current becomes northward. This is the Davison Current or the surfacing of the California Undercurrent. Rosenfeld et al. (1994) emphasized that wind-driven upwelling does not occur within Monterey Bay. That view agrees with earlier work in the bay (Broenkow and Smethie, 1978). Some of the earlier studies on Monterey Bay circulation are summarized in Table 1.

	Upwelling State	Relaxed State	References
Temporal Scale	**1-2 weeks**	**3-6 days**	
Features	Bifurcating upwelling frontal system from Pt. Año Nuevo	?	Rosenfeld et al. (1994); Ramp et al. (1997); Rosenfeld et al. (1995)
	Anticyclonic eddy on the offshore side of the offshore upwelling filament	Anticyclonic eddy moves onshore	Tracy (1990)
	Cyclonic Circulation in the Bay	Cyclonic reduces in extent	Tracy (1990)
	Bifurcating Upwelling frontal system from Pt. Sur	?	Traganza et al. (1981), Tisch and Ramp (1997) and others

Table 1. Circulation Features in the Monterey Bay Region during Upwelling and Relaxed Periods. (From MBARI-BOG: Ten-year Study from Monterey Bay).

Table 1 shows the circulation features in the Monterey Bay with emphasis on the upwelling and relaxation periods. Two areas of coastal upwelling are summarized in the table: one near Point Año Nuevo (Rosenfeld et al. 1994) and a stronger upwelling locus south of Point Sur (Traganza et AL. 1981). These upwelling areas are readily observed in AVHRR satellite images as cool areas.

B. HIGH-FREQUENCY RADAR

1. Characteristics

High-frequency (HF) radio formally spans the band 3 to 30 MHz of the electromagnetic spectrum (with wavelengths between 10 meters at the upper end and 100 meters at the lower end). Throughout the years, oceanography has been exploiting many different portions of the electromagnetic spectrum to build instruments to extract information about the ocean surface, such as altimeters

and scatterometers. There are several types of transmission paths for different frequencies, such as space waves, ground waves, and sky waves. The latter is used for HF radar, in oceanographic applications.

HF radars used in oceanographic applications are surface-based that measure backscatter from the ocean surface on spatial and temporal scales. They are usually located on the coast measuring out from 20 to 200 km depending on the radio wavelength and parameter being measured. The way the systems work can be summarized by the following discussion taken from the Codar Ocean Sensors, Ltd. web site (http://www.codaros.com):

> When the radar signal hits ocean waves that are 3 to 50 meters long (wavelength) that signal scatters in many directions. In this way, the surface can act like a large diffraction surface. Significant radar signal will return directly to its source only when the radar signal scatters off a wave that is exactly half the transmitted signal wavelength, and that wave is traveling in a radial path either directly away from or toward the radar. The scattered radar electromagnetic waves add coherently, resulting in a strong return of energy at a very precise wavelength. This is known as the Bragg principle and the phenomenon 'Bragg scattering.'

The basic mechanism of a HF radar system is the analysis of this backscattered radio wave. HF radar systems work very much like a radio station in that they emit a radio signal. Although a radio station does not monitor the signal that is scattered back to the station, a HF radar site uses this backscattered radio wave to calculate surface currents. Resonant Bragg Scattering basically amplifies the scattered signal directed toward the receiver. Resonance will only occur for a particular signal wavelength:

$$\lambda = \frac{\lambda_t}{2\cos(\theta)}$$

where λ = Wavelength of surface waves; λ_t = Wavelength of transmitted Signal and θ = Incident angle of the Signal.

Since the antennas are very close to the sea level, the incident angle of the signal is assumed to be zero. This assumption reduces the above equation to:

$$\lambda = \frac{\lambda_t}{2}$$

The second equation states that a signal scattered off a wave and back toward the antenna will be in phase with a signal that traveled to the next wave (1/2 transmit wavelength further) and returned to the original wave (another 1/2 transmit wavelength). Therefore, the signal that traveled a whole wavelength further will line up with the first signal. When all of the scattered signals directed toward the receiver are lined up, each signal is added to the other and results in a stronger signal. All the HF radar systems has to do is send out a signal that is twice the wavelength of an ocean wave and the scattered signal directed back to the receiver will be amplified. Because the ocean surface is continually composed of a spectrum of waves, the converse is also true: for any HF broadcast frequency, Bragg-resonant waves will be selected.

All of the above equations assume that the surface waves are not moving. In fact, the waves are moving and a moving wave will change the frequency of the return signal (Doppler shift). The frequency of a signal scattered by a moving wave will be shifted depending on the velocity of the surface wave. If the wave is approaching the receiver, the return frequency increases. On the other hand, a wave moving away from the receiver will return a lower frequency. Therefore the shift will be positive if the wave is moving toward the receiver and negative if the wave is moving away from the receiver. The following equation is used to measure the magnitude of the frequency shift:

$$\Delta f = \frac{2V_R}{\lambda_t}$$

where $\Delta f =$ Frequency shift; $V_R =$ Radial Component of Velocity.

Using linear wave theory one can calculate the velocity of the surface waves. The solution to the above equation will give the size of the Doppler shift for an approaching and receding wave. Note that the magnitudes will be the same with the exception of the sign.

It is important to keep the following in mind: a single radar site is capable of detecting only the component of flow traveling toward or away from the site for a given look angle. A stable estimate requires scattering from hundreds of wave crests plus an ensemble averaging of the spectral returns, which sets the space-time resolution of the instruments. The precision of the system is limited by the frequency resolution of the Doppler spectrum and is typically 2-5 cm s^{-1}. Finally, the accuracy is controlled by numerous factors, such as signal-to-noise ratio, geometry, the position of the antennas, the geography of the location, etc.

What makes HF Radar particularly useful for current mapping is that the ocean waves associated with high frequency wavelengths are always present. Because we know the wavelength of the wave, we also know its speed very precisely from the deep-water dispersion relation. The returning signal exhibits a Doppler-frequency shift. In the absence of ocean currents, the Doppler frequency shift would always arrive at a known position in the frequency spectrum. But the observed Doppler-frequency shift does not match up exactly with the theoretical wave speed. The Doppler-frequency shift includes the theoretical speed of the wave plus the influence of the underlying ocean current on the wave velocity in a radial path (away from or toward the radar). The effective depth of the ocean current influence on these waves depends upon the wave's period or length. The current influencing the Bragg waves falls within the upper meter of the water column (or upper 2.5 meters when transmitting between 4 to 6 MHz; Steward and Joy 1974). So, once the known theoretical wave speed is subtracted from the Doppler information, a radial velocity component of surface current is determined. By looking at the same patch of water using radars located at two or more different viewing angles, the surface current radial velocity components can be summed to determine the total surface current velocity vector.

2. CODAR

CODAR, which stands for Coastal Ocean Dynamics Applications Radar, uses the basic scattering principle for all existing HF radar. The historical timeline of the association of HF radar and its application in oceanography taken from the Codar Ocean Sensors, Ltd. web site is as follows:

> 1955: Crombie discovers experimentally that Bragg scatter produces strong HF sea echo return to first order (Crombie, 1955). 1968-1972: Barrick derives/publishes quantitative solutions for first and second order sea scatter (Barrick, 1968-1972). 1969-1973: Barrick at NOAA (U.S. Dept of Commerce), with Scripps & Stanford, use HF phased arrays on San Clemente Island to validate theories behind HF current and wave measurements. 1973-1983: Barrick leads team at NOAA to develop more practical alternatives to large HF phased arrays for coastal current and wave monitoring (Lipa and Barrick, 1983). Patents were filed and over 100 papers published on CODAR concepts within government.

Nowadays, distinct differences are found in the antenna configurations that transmit and receive the electromagnetic signal. The antenna system utilized by CODAR consist of crossed loops and a whip for receiving and a whip for transmitting radio pulses (Barrick et al., 1977). This type of antenna is used for deployment in populated and rocky coastal areas. The omnidirectional characteristic of the cross-loop whip combination makes it possible to scan wider ocean sectors. These are the types of antennas used in Monterey Bay (Paduan and Rosenfeld, 1996; Paduan and Cook, 1997).

3. Uses

HF radar measurements have been employed around Monterey Bay since 1992. The main difference between the oceanographic radar and other radar, for example those intended to track ships or aircraft, is the operating frequency. Whereas most of the military radars operate at microwave frequencies (wavelength on the order of centimeters), radar uses for oceanographic purposes operate in the HF range with wavelength of tens of meters. This is a crucial issue because the ocean waves interact resonantly with HF radar signals.

With the beginning of operation of HF radars in coastal zones some forty years ago and the application of near-shore current mapping about twenty years ago, it became possible to observe large region of the coastal ocean simultaneously and to construct maps of surface currents, waves, and wind direction.

The uses of the system basically depend on the configuration and the array of the antennas. Horizontal resolution can be from tens to hundred of kilometers. Another characteristic of this shore-based remote sensing technology is that the two-dimensional observations can be collected continuously for relatively low cost compared with others type of systems.

II. DATA COLLECTION

A. MOORED

1. Wind data

*M1 Buoy***:** The importance of time series in oceanographic research is known. Spatial and temporal wind information will need to come from mooring and drifters with arrays of *in-situ* sensors. Realizing that advances in ocean sciences are limited by the lack of instrumentation and systems capable of collecting these time series, the Monterey Bay Aquarium Research Institute (MBARI) established the development of a new set of control, electronics, and software that would allow for the collection, storage and telemetry of data from any of a wide range of scientific instrumentation. The controller name for putting this to work is the Ocean Acquisition System for Interdisciplinary Science (OASIS).

Three different sets of platforms have been deployed by OASIS. For the purpose of this work, we focus on the moored configuration. Buoys with the measurement instrumentation were first deployed at sites M1 and M2 in the waters adjacent to Monterey Bay in August 1989. The sites were selected primarily for scientific reasons and since then the moorings have survived well. The M1 position is the primarily location for the purpose of data collection for this project. The location of the buoy is shown in Figure 1. The data utilized from this platform includes primarily wind data from June 1, 2003 through March 31, 2004.

2. Ocean Data

Bottom Fixed ADCP: These instruments belong to the University of California, Santa Cruz (UCSC) and are part of their program entitled Partnerships for Interdisciplinary Studies of Coastal Oceans http://www.piscoweb.org). The sites are located in relatively shallow waters in the inner shelf. From the three sites, two were analyzed for the purpose of this study: Terrace Point and Hopkins Marine Station. Sand Hill Bluff, which is the third one, is not included as it is too far from the bay.

These instruments are bottom-mounted RDI 600 kHz Workhorse Sentinel ADCP's. The ADCP's sampling interval was configured to be two minutes. The timing was set as Julian days defined as Julian days since 12 a.m. January 1, 2000, Pacific Standard Time. Matlab codes were used to convert between calendar dates and the UCSC PISCO Julian days. The raw ADCP data was converted to text files using RDI's "BBList" program. This program allows for both a tabular display of the data and a conversion to a text format. Because there are too many columns of data to allow the export of just one ASCII file per deployment, two text files are created for each ADCP deployment. In the format there are always 22 ADCP "bins" exported. Hourly averages of each ADCP deployment are also created with site- specific Matlab codes. Because some of the deployments do not have times falling on even minutes, some hourly times do not fall precisely on the hour. Also in the hourly data, bins within six percent of the water-depth of the water's surface, or higher, as determined by a maximum in acoustic intensity "echo," are set to NaN (not a number). Once the data is converted to a text format, it is loaded into Matlab where a minimal amount of processing is done and it is converted into a binary version. Then a set of variables are saved to the original raw file name, but with a MAT extension. For this study, the following are the variables used:

- "Julday": UCSC PISCO Julian day (from 00:00 hrs of 01 January, 2000)
- "eU": matrix holding eastward velocities of all 22 bins, in cm/s
- "eV": matrix holding northward velocities of all 22 bins, in cm/s.

The water depth at the location of the instruments is shown in Table 3 of Chapter III, Method and Data Analysis.

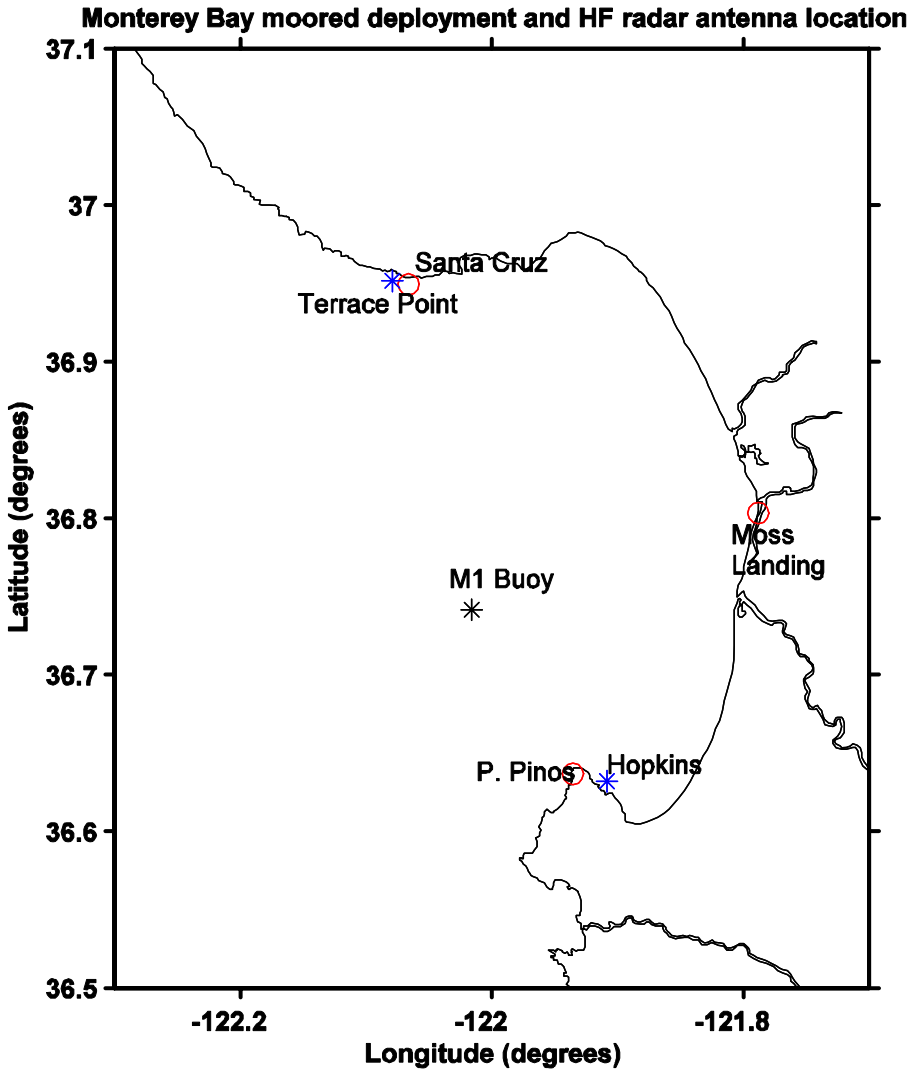

Figure 1. Location of Fixed-bottom ADCPs at Hopkins and Terrace Point and the M1 Buoy (*).

B. HF RADAR DATA

1. Temporal Coverage

Hourly surface currents obtained from HF Radar measurements in Monterey Bay were mapped for the period of July 31, 2003, through March 31, 2004. These HF radar data were obtained from five HF antennas located along the Monterey Bay. The fifth antenna shown in Figure 2, is located in Point Sur, south of Monterey Bay and also helps with radials primarily in the southern part of the bay. Because this antenna is far from the bay, the spacing of the grid was set at five kilometers, in order to obtain a longer range and to reach the southern area of the bay mentioned before. Data were continuously collected every one hour, twenty hours a day during the whole period. For this study, the data were filtered using a 33 hour low pass filter in order to remove the tidal and sea breeze signals.

2. Spatial Coverage

Before examining the spatial coverage, it is important to understand the basics of the configuration of the system. Although the scattering principle is the same for all HF radars, differences are found in the antenna configuration that transmit and receive the electromagnetic signals. Five HF antennas are located along the Monterey Bay, shown in Figure 2. It is important to mention that the geometry of the bay, with a curving coastline with a radius of about 20 Kilometers is ideal for the multisite HF radar network. The over-water distance from one point to another, in this case from Santa Cruz to Point Piños, is close to the typical radar range. When three or more shore locations, which is this case, are used, the entire patch of water can be observed without lost coverage along the baseline between radar sites. This geometry also makes Monterey Bay well suited for validating and developing the algorithm of currents, waves, and wind direction because a large ocean region is over sampled. Even though the fifth HF antennas are located far south of the Bay, its purpose is to help building current map in the south entrance of the Bay. Table 2 shows the position in latitude, longitude, and center frequency of all five HF radar antennas.

Antenna Location	Latitude	Longitude	Center Frequency
Santa Cruz	36^0,949217 N	122^0,0661 W	12.165 MHz
Moss Landing	36^0,803333 N	121^0,7883 W	24.649 MHz
NGPS	36^0,603233 N	121^0,8720 W	13.465 MHz
Point Piños	36^0,636783 N	121^0,9356 W	13.195 MHz
Point Sur	36^0,30580 N	121^0,9013 W	13.467 MHz

Table 2. Position and Frequencies of HF Radar Antennas along Monterey Bay.

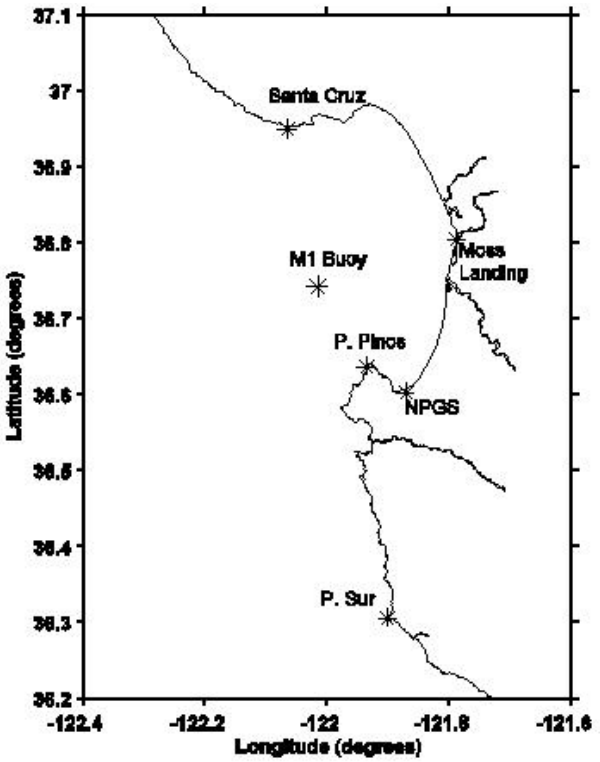

Figure 2. HF Antennas Location around Monterey Bay.

3. Vector Surface Current Maps

A software system named HFRadarmap has been developed at the Naval Postgraduate School using MATLAB codes with input from a number of additional HF radar users around the world. For this study, the main purpose of the HFRadarmap toolbox was to combine HF radar-derived radial currents into total current vectors. Also, the program computes statistics on the total current data and provides radial and total current animation capabilities. The most important goals of the HFRadarmap toolbox are to provide platform independent programs that are not specific to any HF hardware and to make them modular and flexible and easy to use. The system processing streams basically consist of three data products: the backscatter spectrum, or cross spectrum, radial current maps, and total current maps. The primary use is to convert radial currents into total currents and in this way to view total and radial current animations. Since the HFRadarmap software allows the user to process their own total current maps, it gives the user the flexibility to vary the parameters, such as the temporal or spatial averaging values. It also provides flexibility in plotting and saving the total current.

To get from radial to total vector, it is important to mention that a radial current is the component of the total current either directly toward or directly away from the measuring HF radar. Two or more collocated, or nearly collocated, radial currents can form a system of equations that can be solved for the *u* and *v* components of the total current.

C. REMOTE SENSING

1. Satellite AVHRR

Images from satellite AVHRR were obtained to provide another source of information. The following satellite images were obtained from a presentation during a second field test for the AOSN (Autonomous Ocean Sampling Network) program where researchers gathered at MBARI during the summer of 2003 for a month-long experiment to study upwelling features in the Monterey Bay. The

original downloading and processing of the sea surface temperature (SST) and ocean color images was accomplished by MBARI and UCSC.

Figure 3 shows a set of four SST images on different days with a patch of low-temperature waters in the northern area entering to the Bay. This is the typical development of an upwelling event caused by the wind stress blowing continuously from the northwest, resulting in the rise of colder waters from below and the replacement warmer surface waters close to the coast.

Figure 4 depicts a current map from HF radar data of August 10. The wind speeds during the time of these observations had some of the largest magnitudes during the course of this study associated with the upwelling event between August 8 and August 18. The majority of the wind direction is from the northwest and the surface currents align with the strong wind blowing toward the southeast. Figure 5 shows this major upwelling event developed between August 8 and August 18 (marked with an arrow) the wind blew continuously from the north for at least ten days and the satellite image probably shows the beginning of the transport of colder waters from the bottom to the surface. Further analyses are discussed in Chapter III, Method and Data Analysis.

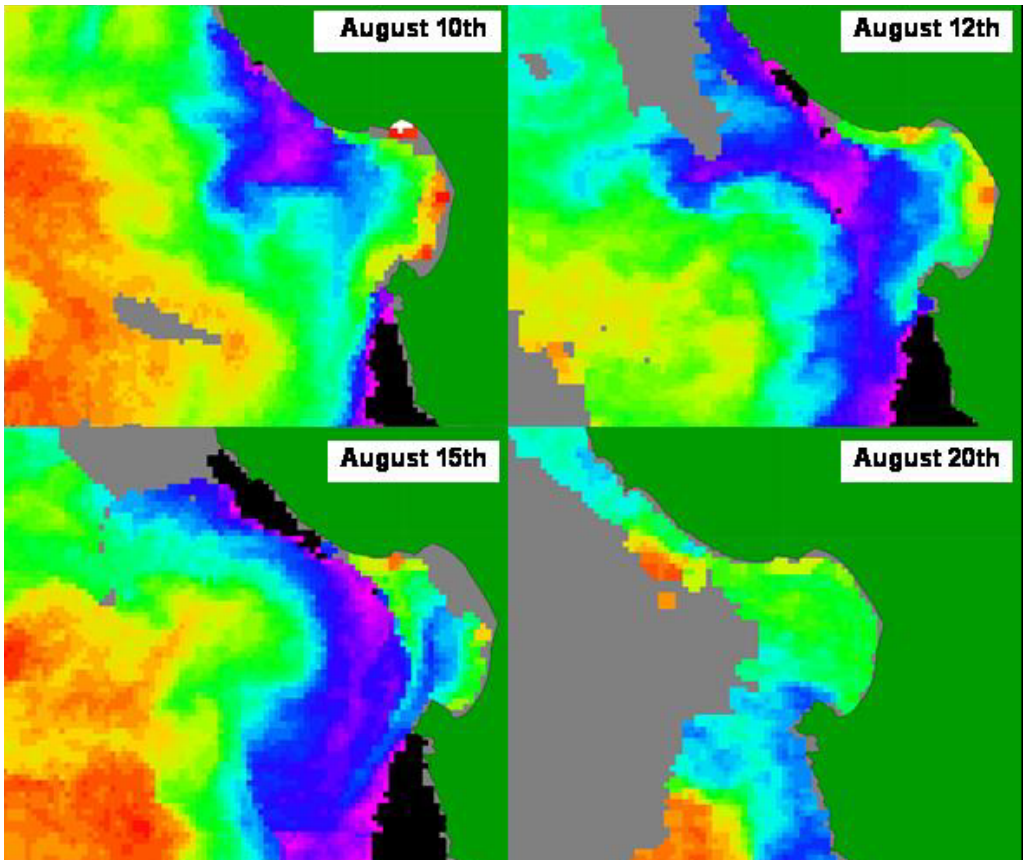

Figure 3. Satellite AVHRR SST images for August 10, 12, 15 and 20, 2003, respectively. (Courtesy F. Chavez).

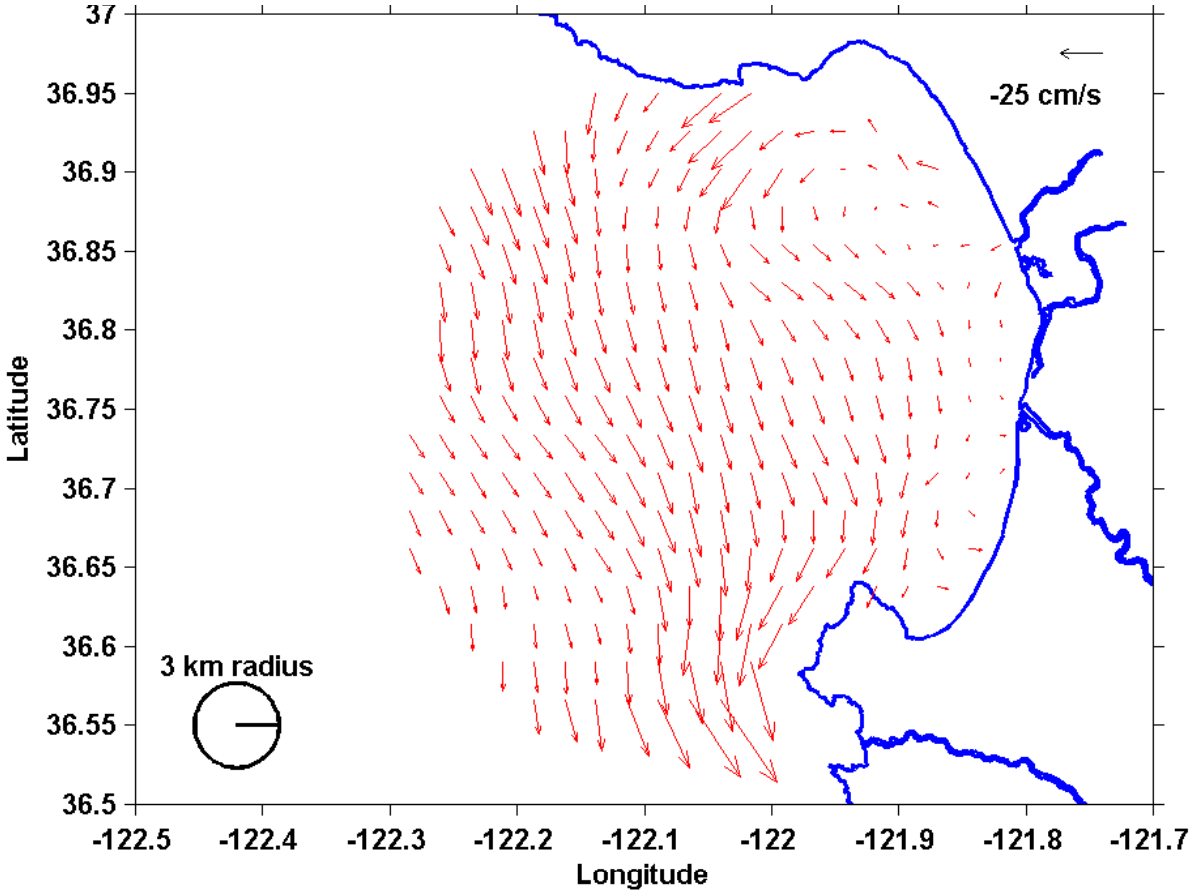

Figure 4. HF Radar-Derived Surface Current Map of August 10, 2003.

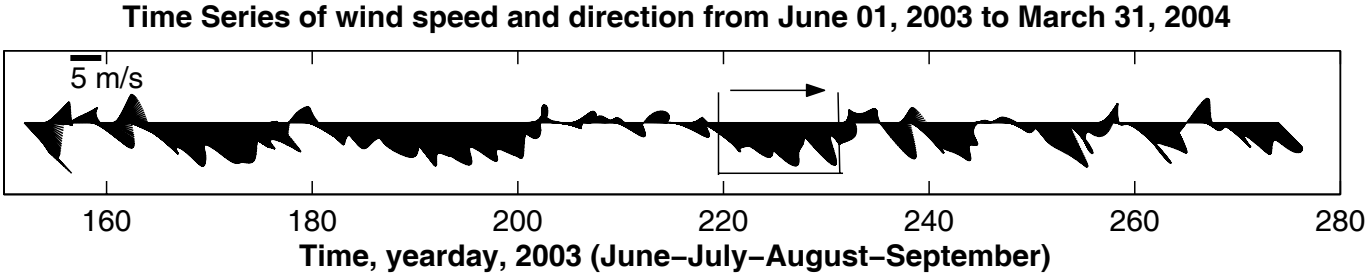

Figure 5. Feather plot of low-pass-filtered wind vectors at the M1 mooring showing major Upwelling events from June to September, including the highlighted period of 8-18 August.

2. Aircraft IR

Data collected from an aircraft were also analyzed. The data was obtained in collaboration with CIRPAS, the Center for Interdisciplinary Remotely-Piloted Aircraft Studies. This center was established by the Office of Naval Research in the spring of 1996 to provide Unmanned Air Vehicle (UAV) flight services to the research, development, test and evaluation communities. The Naval Postgraduate School's Center is located at the former Fort Ord's Frizsche Field (Marina Municipal Airport). CIRPAS operates a variety of manned and unmanned vehicles; one of those is the Pelican OPV. Pelican was developed to meet an optionally piloted aircraft requirement to perform long endurance low-altitude atmospheric and oceanographic research and technology development. The aircraft is a highly modified Cessna 337/O-2A Skymaster with all the equipment and instrumentation necessary to support user requirements.

Data to construct the SST, wind and reflectance data, were collected at an altitude from 30 to 400 m over the Monterey Bay. The following plots (Figures 6, 7, 8, and 9) depict sea surface temperature from the true trajectory of the plane. No gaps are filled out, so the data collected is the real SST from the aircraft path. The number above each plot indicates the year, month, and day the data were taken. As an example, SST 030713 means Sea Surface Temperature of July 13, 2003. The analysis of these plots is in Chapter III, Method and Data Analysis.

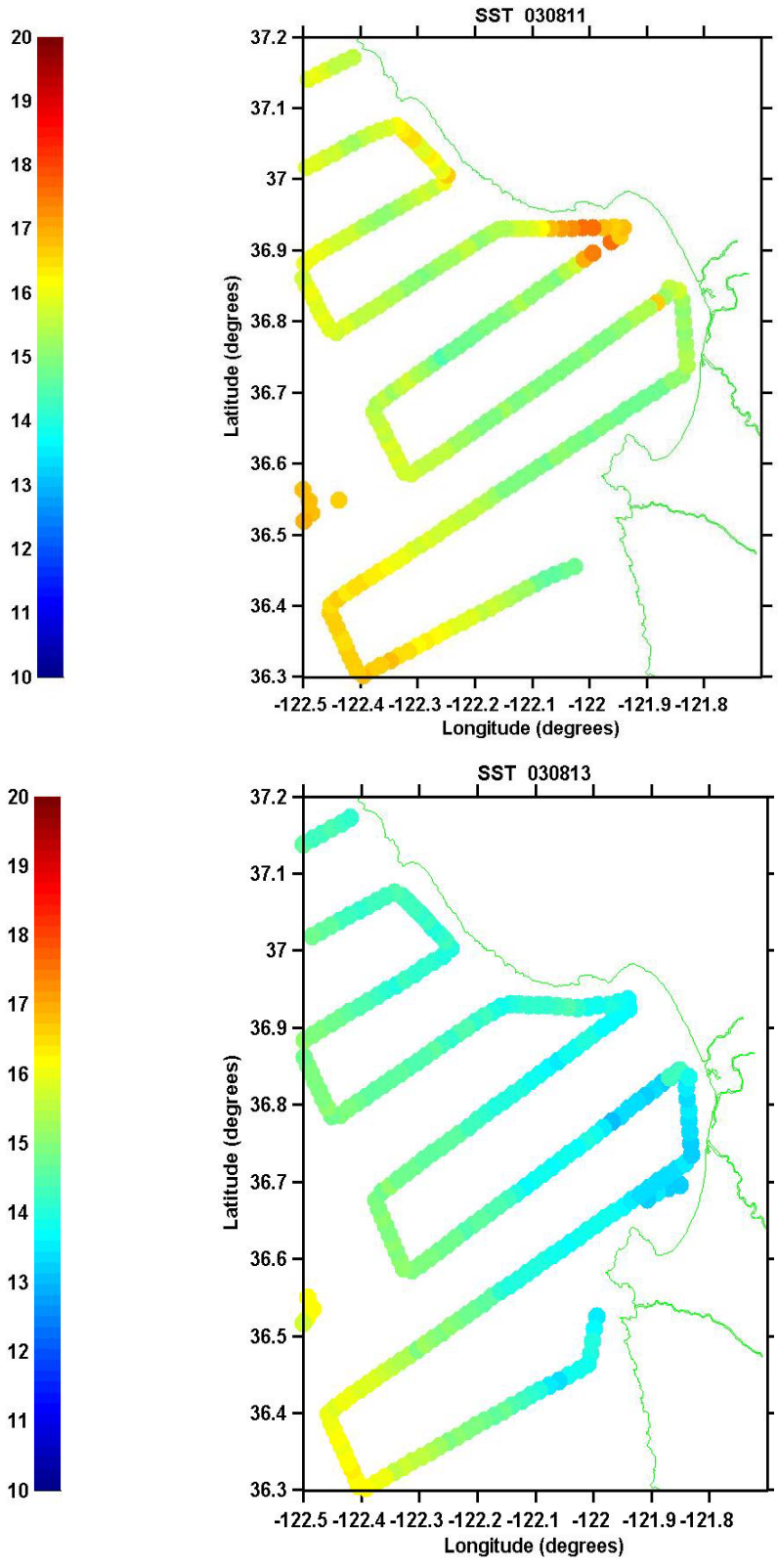

Figure 6. Sea Surface Temperature Pattern taken from Aircraft in Monterey Bay (August 11and 13, 2003).

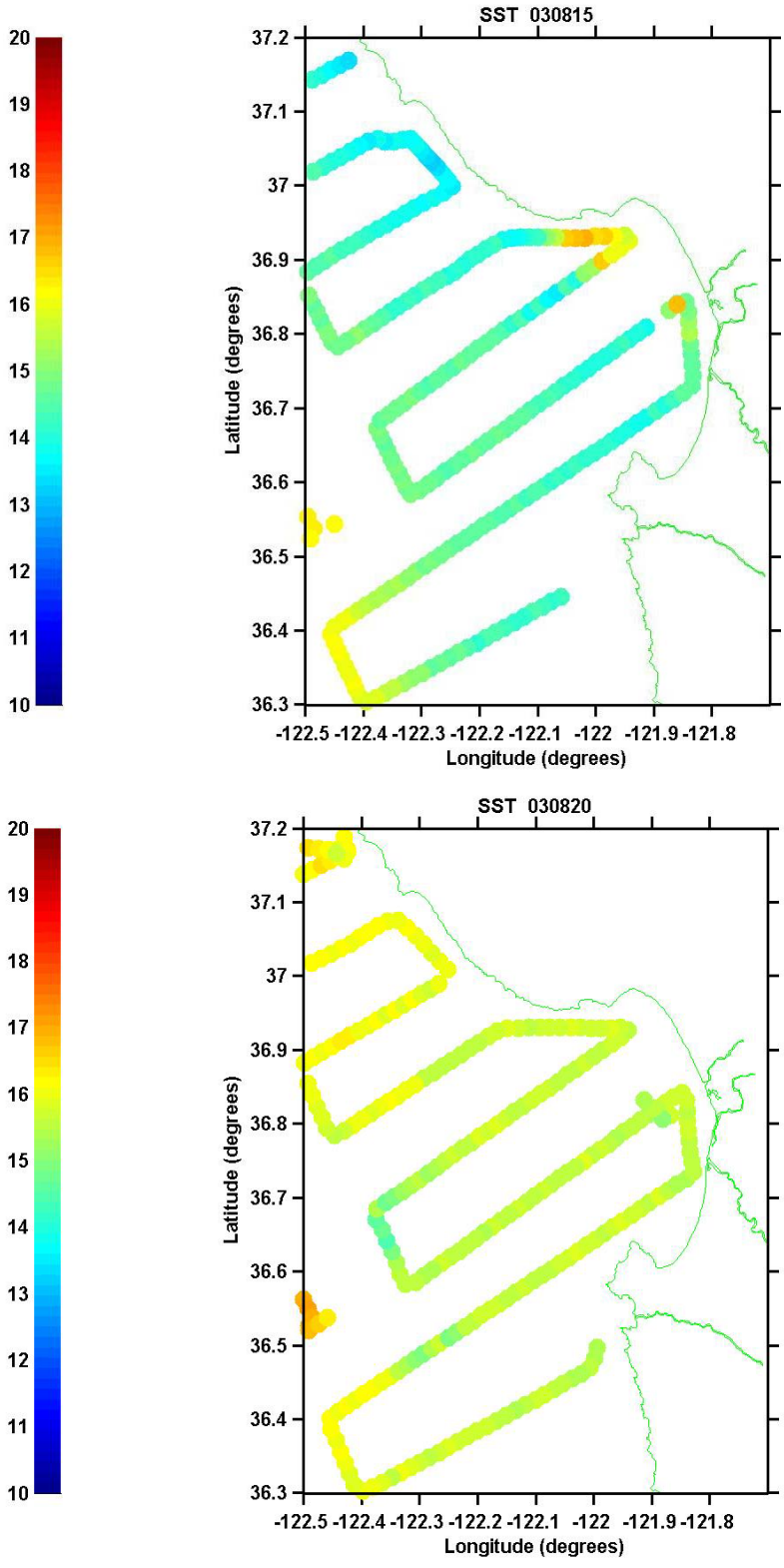

Figure 7. Sea Surface Temperature Pattern taken from Aircraft in Monterey Bay (August 15 and 20, 2003).

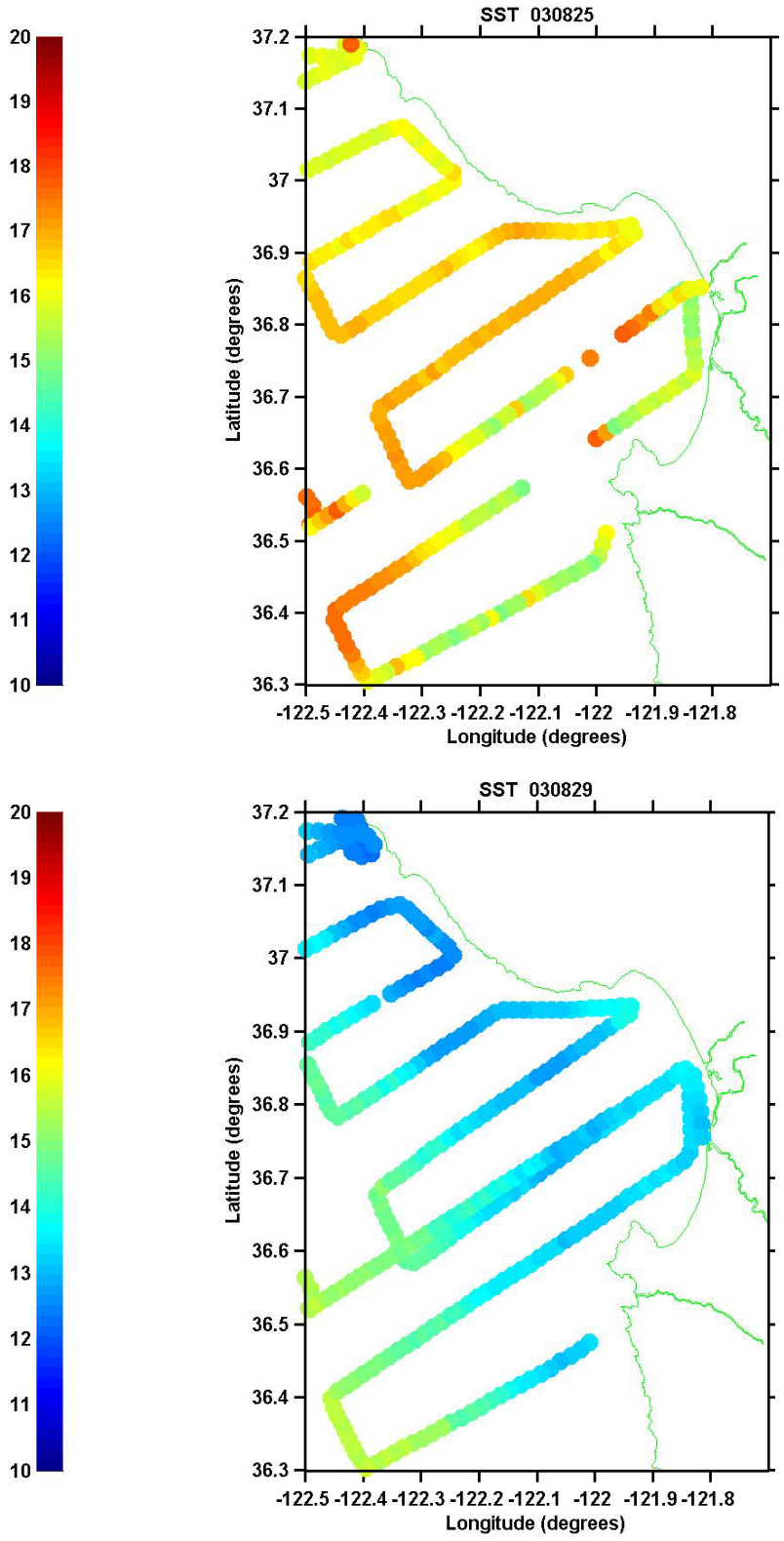

Figure 8. Sea Surface Temperature Pattern taken from Aircraft in Monterey Bay (August 25 and 29, 2003).

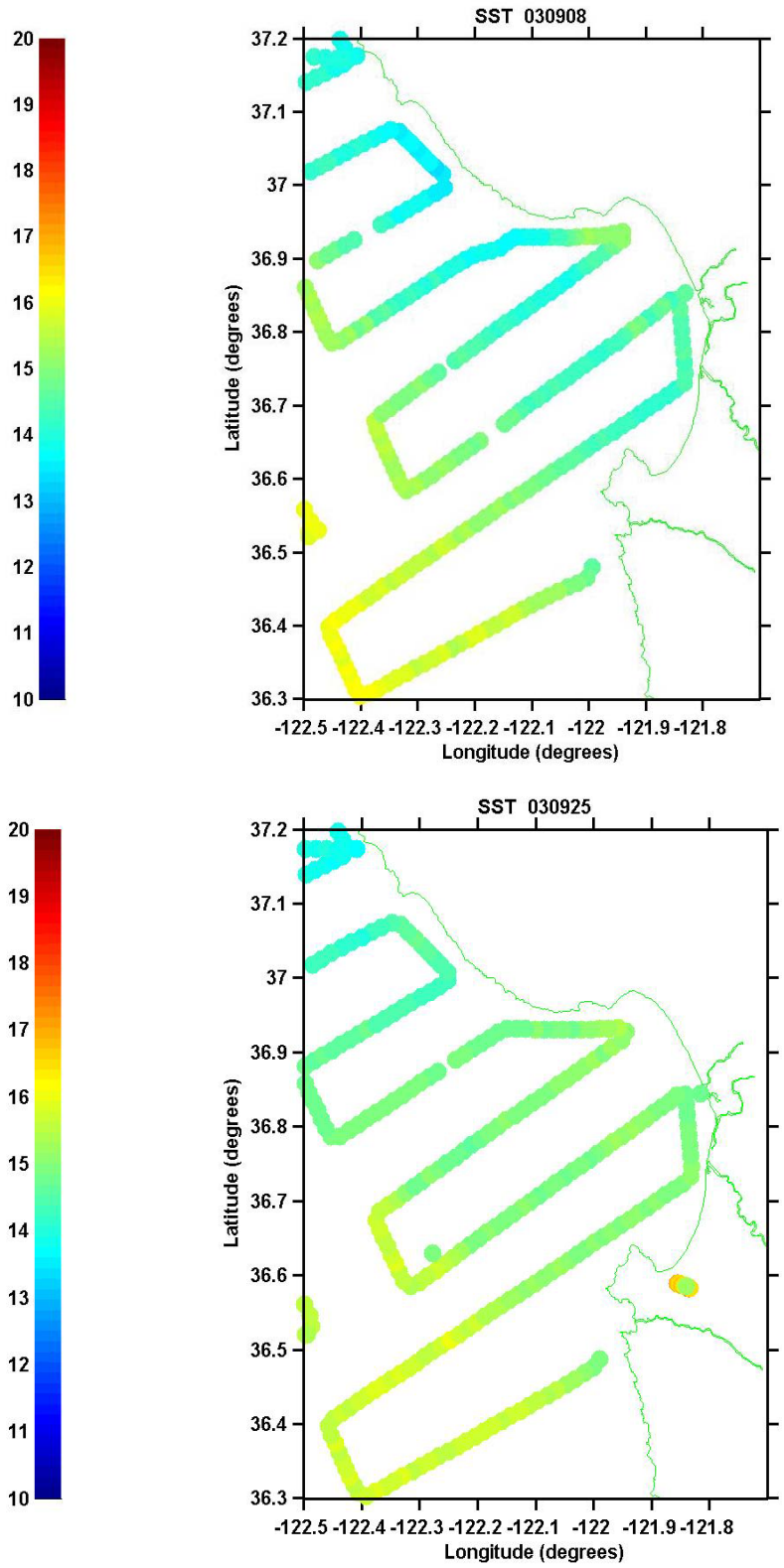

Figure 9. Sea Surface Temperature Pattern taken from Aircraft in Monterey Bay (September 8 and 25 , 2003).

III. METHOD AND DATA ANALYSIS

A. HF RADAR MAPPING PROCESS

Hourly surface currents in Monterey Bay were measured continuously from June 1, 2003 to March 31, 2004 by a network of five HF radar antennas of the CODAR type. The measurements were averaged over one-hour intervals and the total surface velocities were reported on a grid with a uniform spacing of about three kilometers. The data used was filtered to eliminate the diurnal and semidiurnal tides and local wind variations. Time and space gaps in the radar measurements were filled using linear interpolation. The interpolation criterion required that data was available at least 75 % of the time. Figure 10 shows the total grid coverage in Monterey Bay. Before proceeding to the next step, it is necessary to briefly mention some of the concepts involved in the data processing.

The data products produced by the HF radar equipment are cross spectra based on the radio wave backscatter, radial current maps derived from the cross spectra each hour, and total current maps, as mentioned before. The cross spectral data must be processed with a direction finding algorithm to produce a radial current map, depending on the type of hardware and on the method used to gather the spectrum. Once the raw backscatter data has been converted to a radial current map, it is hardware independent. All that is needed to describe a radial current would be the location, and the speed and direction of *u* and *v* components.

It should be noted that the output radial format of the radial current maps for different HF radar manufactures is not standard. There are differences in both file formats and in the interpretation of the direction. In some cases movement toward the radar site is stored as a positive value while in other cases it is considered to be negative. To avoid these issues, the MATLAB-based HFRadarmap toolbox developed at NPS produces a standard ASCII format for the radial map data. This consists of 1 row of 4 values in the file, the longitude

and latitude of its location, and the *u* and *v* components of the radial flow expressed as a vector. Using *u* and *v* in this way, the position and direction are unambiguous.

As a reminder, a single data station measures only the component of flow along a radial beam emanating from the site; therefore, radial current from two or more sites must be combined to form the vector surface current. For Monterey Bay, five are the sites combined to get the radial vectors for each of the antennas sites and finally the mapping of the total current as a result of these five antennas. Figure 11 is an example of the radial vector of two antenna sites along the bay. The Moss Landing range of the vectors is shorter than the other sites. This is because the frequency of the transmission at that site is higher that the others (~24 KHz for Moss Landing vs. ~13 KHz for the others); therefore, one achieves less range and better resolution. Also the radial vector coverage at NPGS site is masked to the right due to the geography of the coast.

Figure 12 is the result of the combination of the radial vector of the different antennas. A surface-current map is depicted as a result of the combination of more than two sites, which have combined to form the total surface.

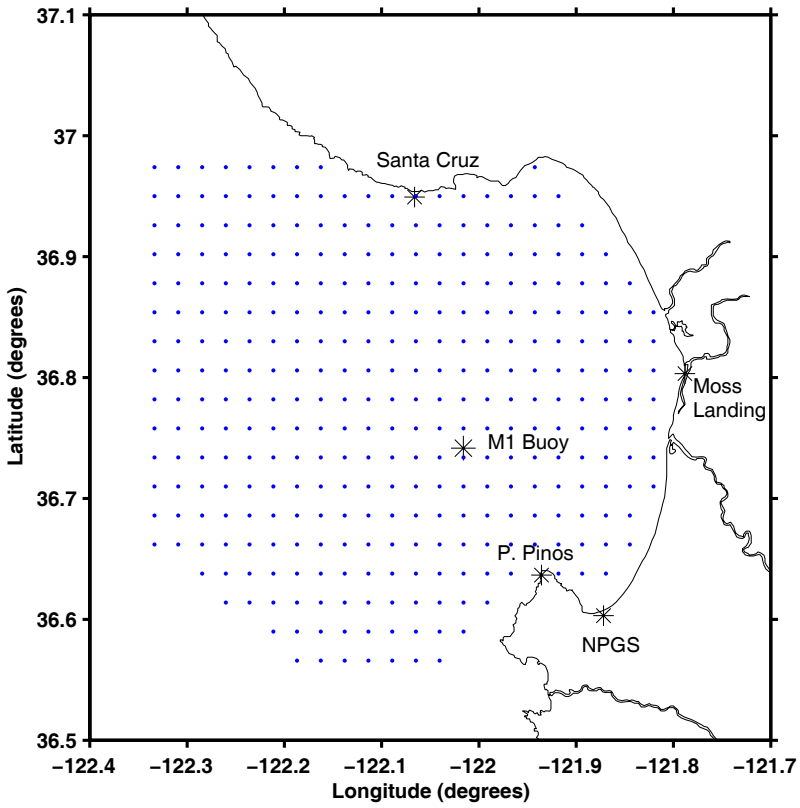

Figure 10. HF Grid Points Coverage in the Bay and the Antenna Location and M1 Buoy Location.

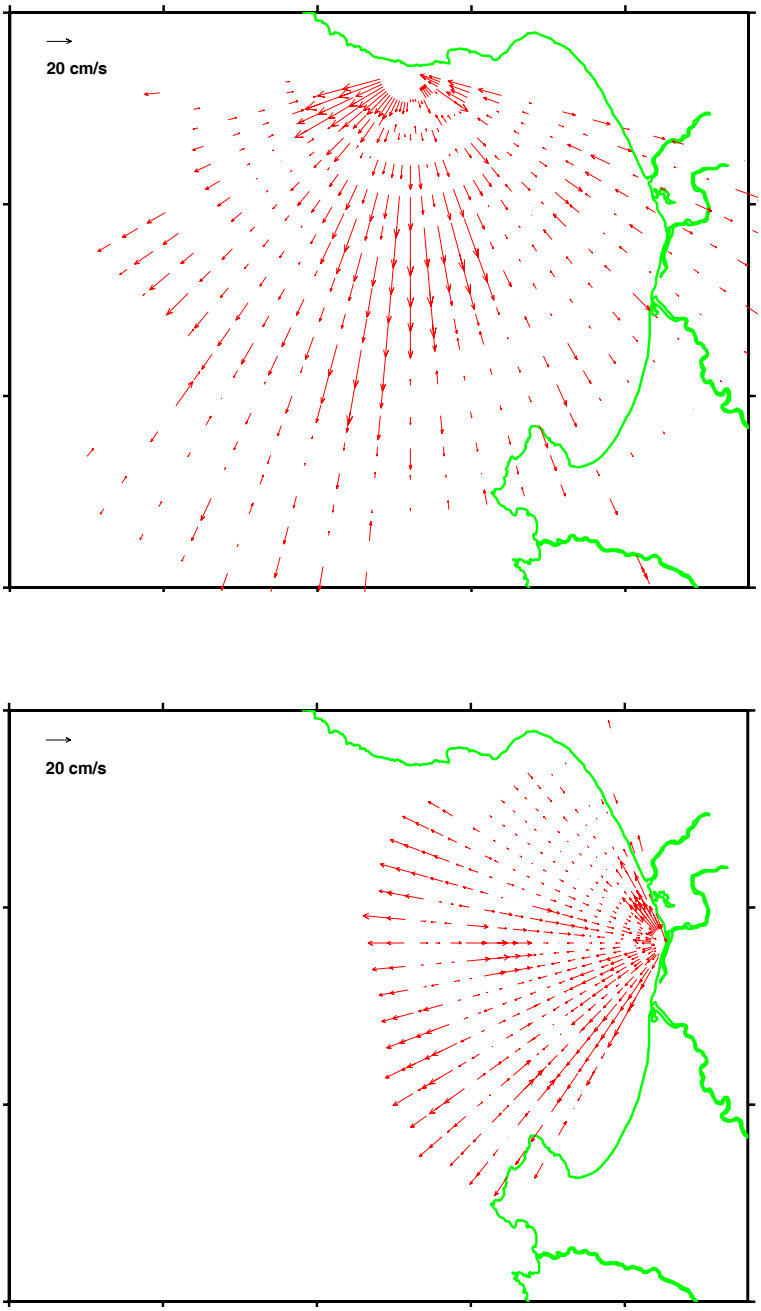

Figure 11. Examples of Radial Vector of two HF Radar Antenna Sites. First one corresponds to Santa Cruz. The second one to Moss Landing.

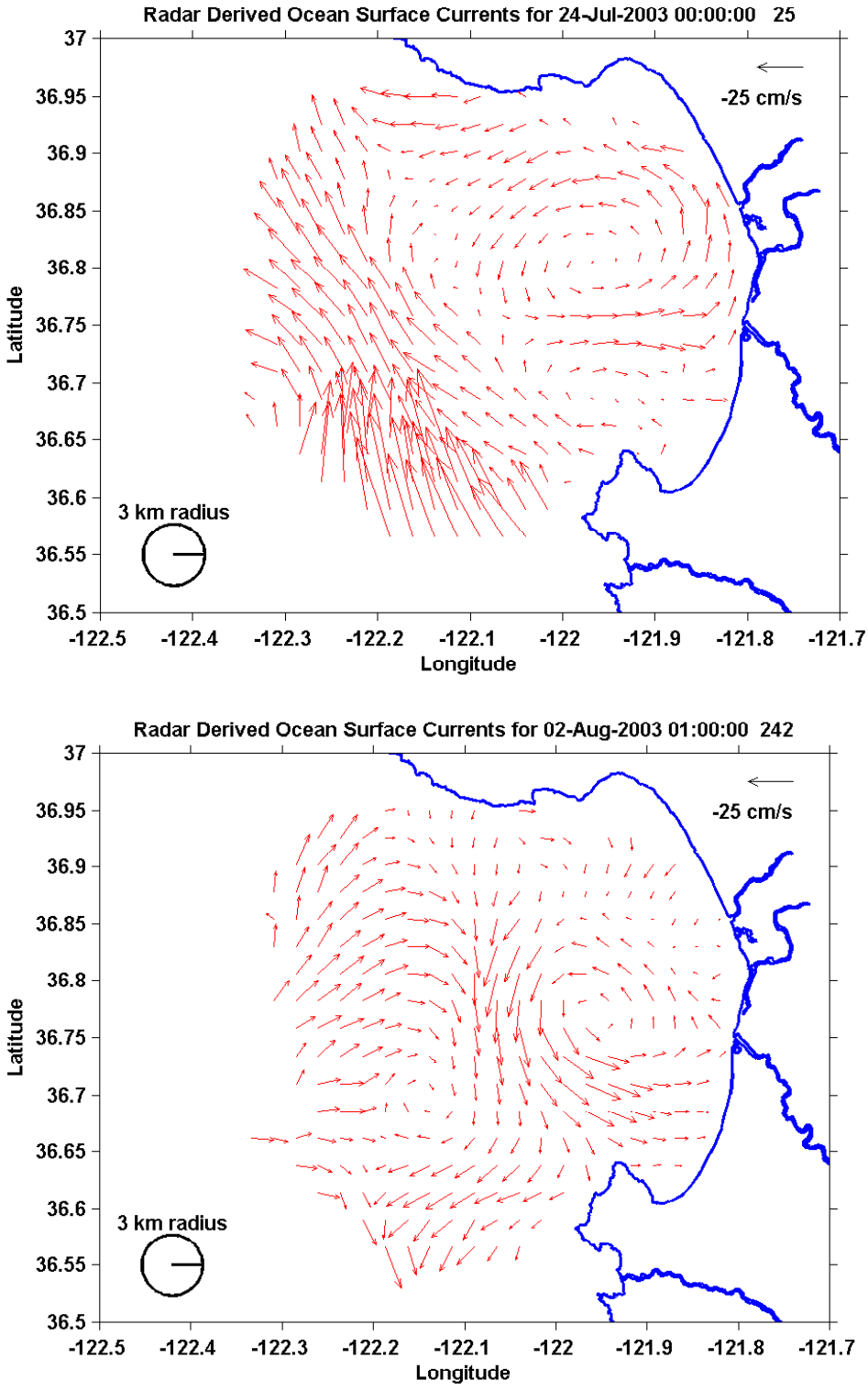

Figure 12. Example of Surface Current Maps of Monterey Bay from the HF Radar Network for July 24, 2003 and August 2, 2003 respectively.

B. MOORED INFORMATION

Moored surface wind information was obtained from the MBARI buoy positioned at the location named M1 as shown in Figure 10. The other moored observations that were analyzed were the information of the *u* and *v* velocity components from the PISCO Bottom-Fixed ADCP instruments. These instruments were located close to Santa Cruz and Point Piños. Table 3 describes the location and some characteristics of the instruments. In this study, data from Sandhill Bluff was discarded from the analysis because the location was too far from the bay.

The purpose of the analysis of the surface currents obtained from the ADCP instruments is to gain another source of information and to relate or to compare these results with the results of the total currents vector from the HF radar grid points. One must consider that the position of the bottom-fixed ADCPs are very close to the shore and the current component computed by the instruments were taken from one specific depth “bin” from a total of 22. This was done to obtain just the information of *u* and *v* components as close to the surface as possible. By comparing the ADCP data from all 22 “bins” from the bottom to the surface, “bin” number 13 was chosen to be the best available near-surface bin. This bin takes the information of the current at approximately four meters below the surface. Information from bins closer to the surface was discarded because the data were not of sufficient quality due to the tidal and waves dynamics and to the direct-path acoustic reflections from the sea surface.

The data from the bottom-fixed ADCPs cover a period of time that is limited compared with the longer HF radar record, as shown in Table 3. Only the summer time period was analyzed with respect to the bottom-mounted ADCP data.

When data obtained from the HF radar network and from the bottom-fixed ADCP instruments are compared and correlated, it is necessary to point out the fact that the position and horizontal extent of the instrument's coverage are not the same, even though they may be relatively close together. The differences in

the positions will lead to real differences in the velocity data. Another issue is that the information collected by the HF radar antennas were taken from the very skin of the water surface (within 1 m) while the data from the ADCP was at about 4 m depth.

Name	Location	Meters above Bottom	Period of Collected Data
Terrace Point	122^0,0803 W 36^0,9442 N	20 m	July 22 - Sep 22 2003
Hopkins Marine Site	121^0,8937 W 36^0,6091 N	18 m	July 31 - Oct 23 2003
Sandhill Bluff	122^0,1578 W 36^0,9728 N	18 m	July 25 - Oct 28 2003

Table 3. Identification of the Bottom-Fixed ADCP Instruments.

C. SATELLITE AND AIRCRAFT DATA

Figures and plots from Chapter II, Data Collection, depict SST taken from aircraft and satellite images. The SST images in Figure 3, show four stages of incoming low-temperature waters in the northern area, entering the bay. These processes represent the consequence of a sustain wind stress blowing from the northwest. A plume of cold waters rises to the surface, replacing warmer waters. This is depicted in images dated on August 10, 12 and 15. The last image dated on August 20 shows how the cold-water plumes are moving away to the south and warmer waters are again appearing in the Bay. This is because the northerly wind stress stopped blowing by yearday 232; this is on August 20 as is roughly shown in Figure 5. Figure 4, a total-current map, shows how the surface current flows toward the south, due to the persistent wind depicted in Figure 5. The wind blows continuously from the northwest between August 9 and August 19, 2003, so the satellite images show one of the major upwelling events that developed in that period.

Figures 6 to 9 depict the aircraft SST data over the bay. The first of the figures, SST from August 11, shows relatively warm temperature around the Bay, in the upper plot and two days later, in the lower plot, colder temperatures run from into the Bay to out of the Bay. This is consistent with the satellite images showing colder waters covering the Bay during the same period of time. The upwelled waters are replacing warmer surface waters due to the constant wind stress.

Figure 7 shows the continuity of cold waters in the upper plot. In the lower plot, dated on August 20, about two days after the wind stopped blowing, SST becomes warmer again. A relaxation period began for just a few days with a shift in the direction, but it was very weak. Figure 8, August 25, shows warm surface waters in the entire bay area. After the brief relaxed period, the wind started blowing again from the northwest between yearday 238 to 245, according to Figure 5. This is from August 26 to September 02, with a reversal in the wind direction in the middle of the period. The plot below shows again the characteristic of an upwelling situation with cold waters circulating out of the bay in the same way as the plot of Figure 7. Figure 9 shows in the first plot, relatively cold water which probably started to get colder due to another wind stress event from the northwest from approximately September 7 to September 12. The last plot, September 25, shows warmer waters and is consistent with a period of reversal of the wind on that date according to the feather plot of Figure 5. All the above descriptions - periods of upwelling, relaxation and reversal of the wind of August and September - can be seen in more detail in Figure 13, which depicts those events in a stick plot of direction and intensity of the wind for that period.

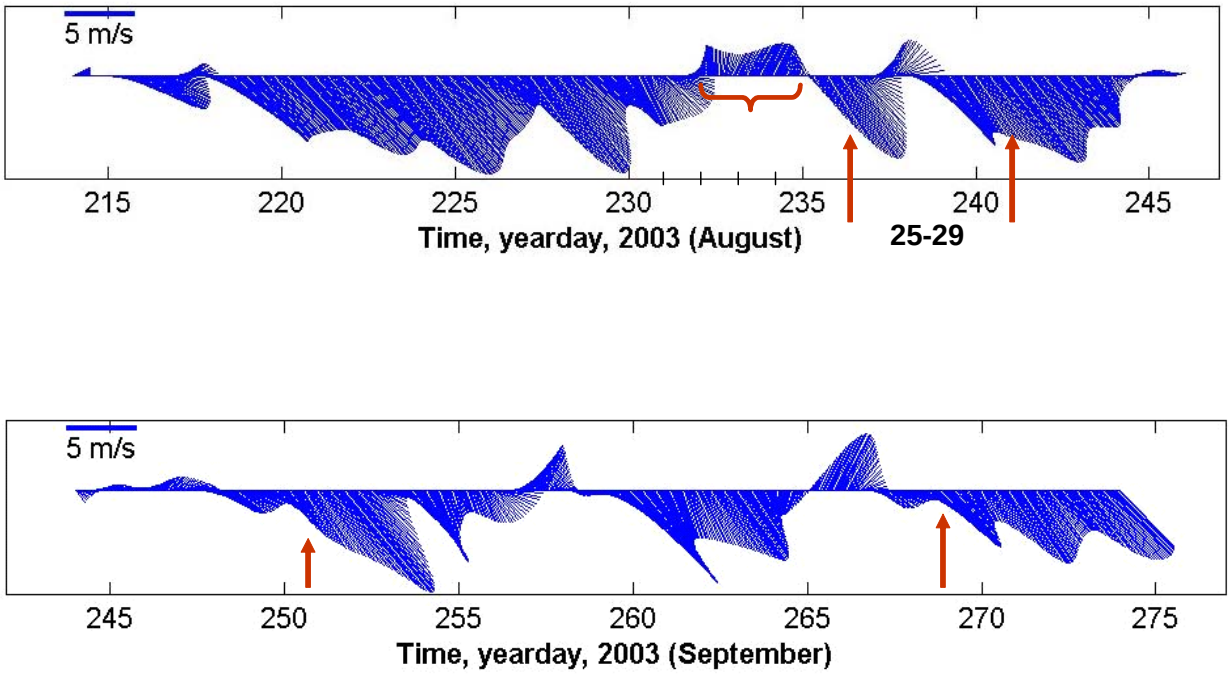

Figure 13. Wind Speed and Direction of August and September, respectively, at the M1 mooring highlighting major Upwelling Favorable Wind and Reversals Conditions.

D. TIME SERIES

1. Wind Data from the M1 Buoy

The plots in Figures 14 and 15 show the time series of the wind component from the M1 buoy for the period from June 1, 2003 to March 31, 2004. The wind data were low-pass-filtered in the same manner as the HF radar-derived surface currents using a Matlab code to eliminate the diurnal wind effects. (One must note that Figure 15 includes four months in the time series of the first plot. The two plots below contain three months per plot, so the scale of the feather plot from one row to the other is different.)

From Figure 14, which depicts the time series of the whole period, the different events of upwelling condition, relaxation periods, and reversals of the wind with downwelling condition are clear. The wind stress lasting for a certain period of time is interrupted by a shorter period of relaxation. Winds blowing from the north-west (pointing to the southeast, according to the stick plot) that correspond to the upwelling favorable wind conditions are much more notorious than the periods of wind blowing in the opposite direction or downwelling conditions. This is more noticeable during late spring, summer and the beginning of fall (from mid-June to late November). After this period, clear winter events are shown from mid-December to February. Relaxation periods are quite brief, lasting just a few days, even just hours, until the wind shifts to another direction.

A MATLAB program was created to analyze the behavior of the surface current related to the wind stress using the M1 Buoy wind data and relating this information with the data from HF radar maps through the use of conditional averaging. The main idea is based on knowing the different wind conditions and then determining what the surface currents looks like under certain types of wind intensity and direction. For example, how do the currents respond after a main wind event taking into account the wind speed and direction plus the duration of that condition? The MATLAB program works by identifying the times of the wind record that meet the user's specified conditions. The user is allowed to input an angle wedge, minimum current speed, duration of this condition, and number of hours after the event starts and a stop-time to end the event. The winds meeting

these criteria are used to determine the times for which to average the HF total currents. The resulting output includes a stick plot indicating wind speed and direction during the selected time periods and maps of the conditionally averaged HF radar-derived surface currents along with their standard deviation and standard errors of the mean.

As an example: The wind is blowing at 5 m/s or more in an angle between 270^0 to 350^0 and the time to wait before the program starts averaging current maps is set to 24 hours. The latter waiting period is referred to as the spin-up time. In this example the program would search the wind record and pick the wind observation times for which the wind was blowing 5 m/s or more in the selected angle range. It will then eliminate those wind events whose duration is less than the specified spin-up time. So, in this example, an event must have 24 hours in the speed and direction conditions before times are selected for averaging the HF radar maps. The event cutoff time is the first time after the spin-up time for which the speed and direction conditions fail to be met. Then the program picks all the current maps that fall in event periods and averages them together. The goals of this analysis are to try to identify recurring surface current patterns and to determine how long it takes for the surface current patterns to respond to changes in the wind stress forcing.

From Figures 14 and 15, which show the ten-month vector wind time series, the main events related to upwelling favorable wind conditions and to downwelling or relaxation periods are depicted. However, to help make an objective decision about which are the major events during the ten-month period of this study, histograms of the speed and direction of the winds at the M1 buoy are depicted in Figures 16 and 17. In terms of wind direction, the lower panel of Figure 16 and the wind rose in Figure 17 clearly show the predominance of upwelling favorable winds blowing from about 310 degrees. Wind speeds were observed to vary more broadly from about 1 m/sec to 9 m/sec with peak occurrences around 3 m/sec.

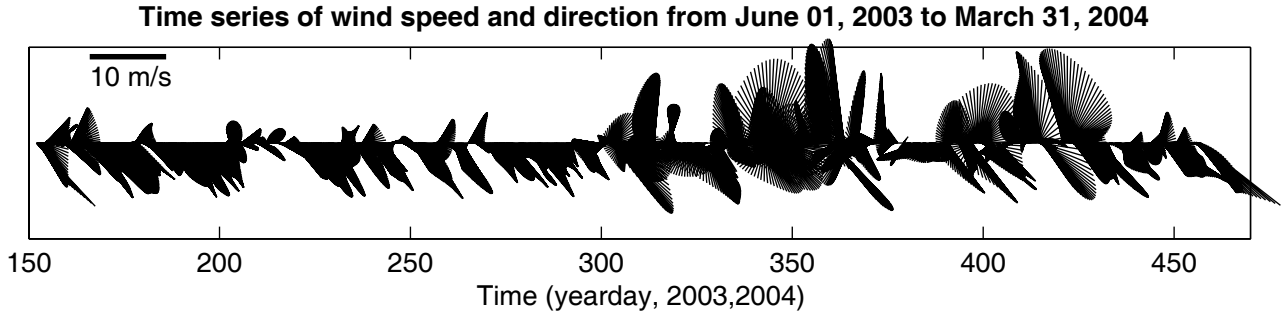

Figure 14. Wind Speed and Direction from M1 Buoy from June 01, 2003 to March 31, 2004.

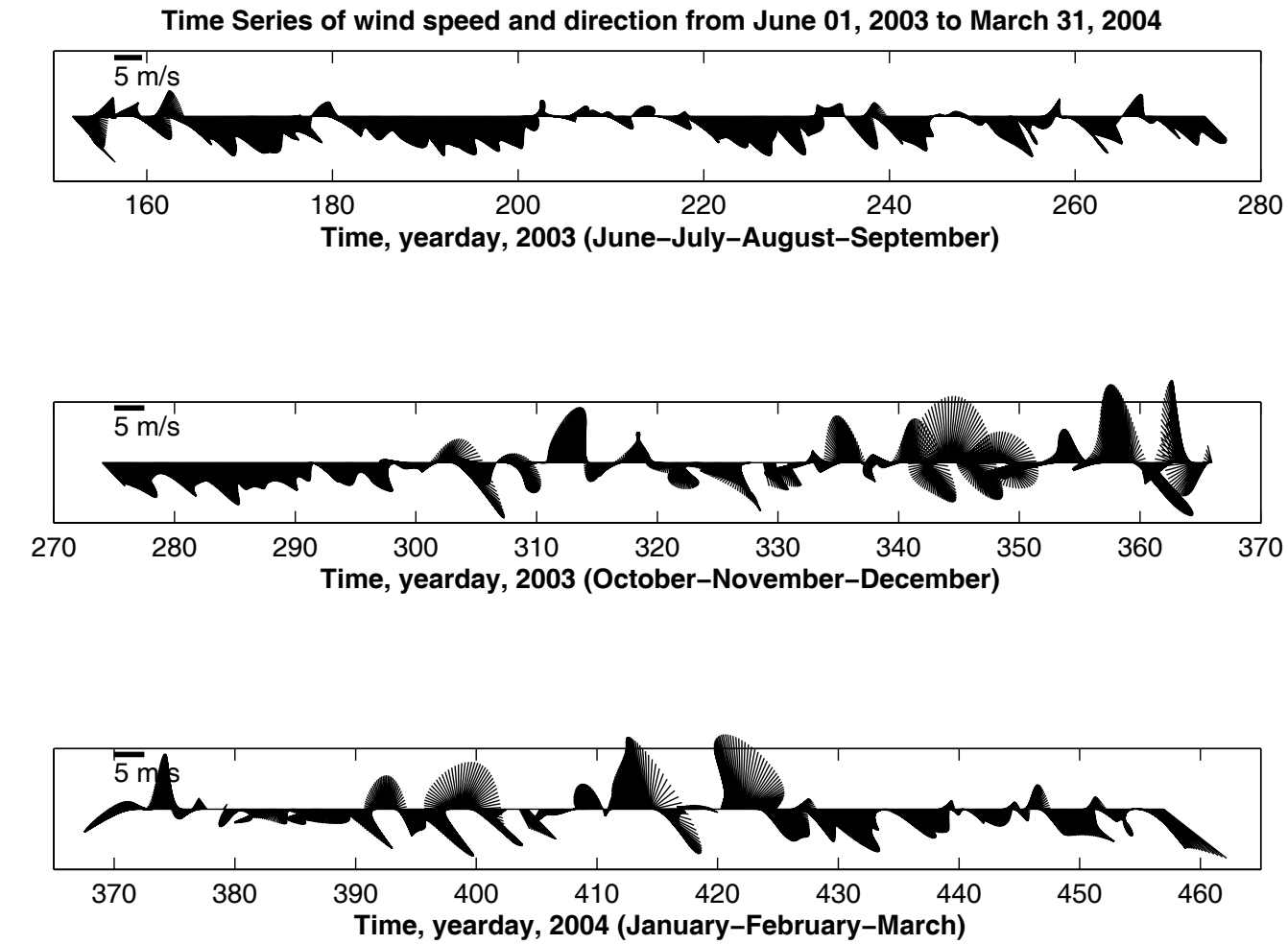

Figure 15. Wind Speed and Direction from M1 Buoy separated by month periods.

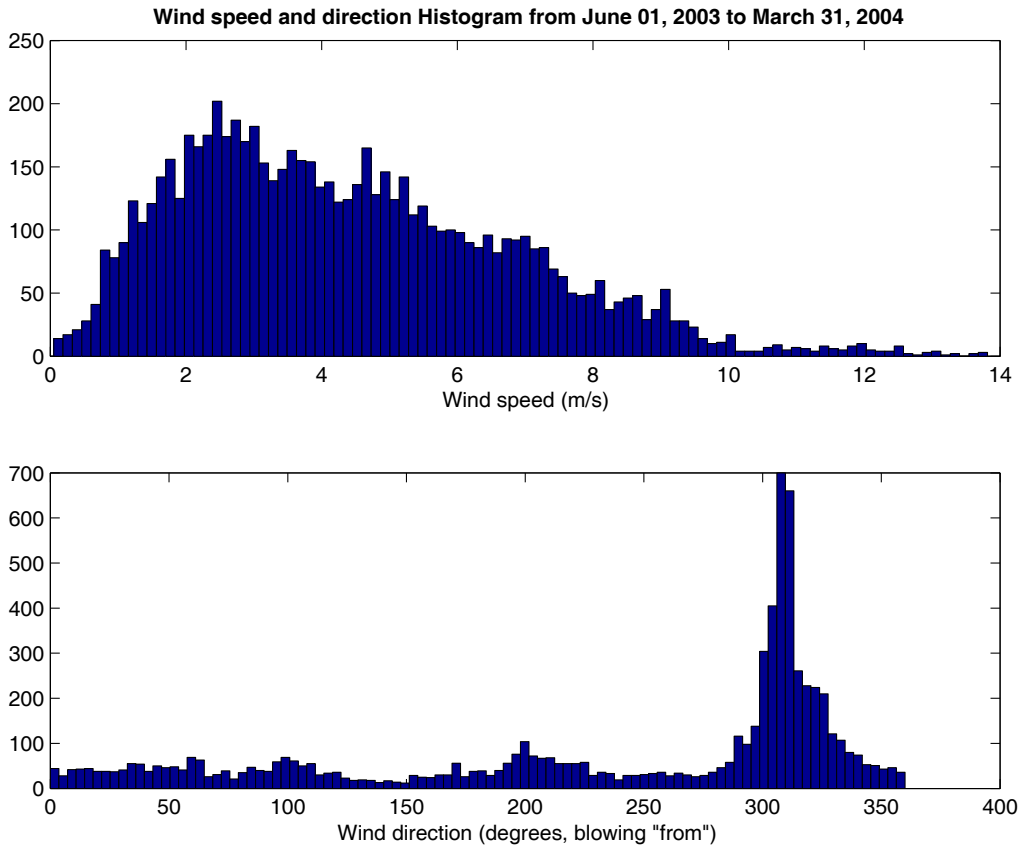

Figure 16. Wind Intensity and Direction Histogram of the Period of June 1, 2003 to March 31, 3004.

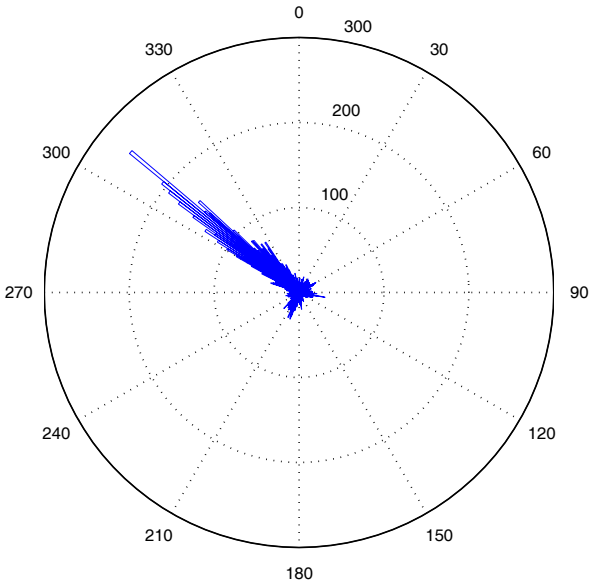

Figure 17. Wind Direction Rose Histogram (bins depicts direction of the incoming wind).

2. HF Radar Map

Several different wind conditions were chosen to analyze with respect to the surface current response to the wind stress and wind stress variability. These several case study events are depicted in Figures 18 to 33. In each figure, there are three separate plots. The first one corresponds to the wind intensity and direction of the whole period. The darkly colored vector time periods represent the times when the particular user-input conditions, the minimum wind speed, the wind direction, and the spinup time, were met by the observed winds. The second plot depicts the conditional mean of the surface currents during all of the selected times based on the wind criteria. The third plot shows the conditional standard error of the mean defined by:

$$\text{Standard error} = \frac{2 \times sd}{\sqrt{N/33}}$$

where: sd = Standard deviation

N = Number of samples.

The total number of hourly samples is divided by 33 because of the low-pass filter used on the data. The greater the number of hourly current maps included in the averages the lower is the standard error. As a result the setting of a certain condition of wind speed, wedge angle, and spinup time results in a low number of observation times that meet the criteria, then the standard error would be bigger than if the conditions are met more often.

Analysis of the different conditions:

a. Upwelling

Most upwelling favorable wind occurs with the wind blowing from the northwest, as shown in Figure 14 and Figure 15. From the histograms of Figure 16 and 17 most of the direction of the wind comes from 310^0–320^0. Since all major events should be represented, the angle wedge used was between 300^0 - 350^0. A wider angle range was chosen to give more chances of upwelling winds conditions. The minimum wind intensity was set to be 4 m/s. With this

angle and wind speed, we select the most obvious features in the HF radar current maps.

The spin up time for most of the cases was set at 12 to 24 and 48 hours. Again, this means that for this condition, the wind will be blowing uninterrupted at a minimum of 4 m/s from a wedge angle between 300^0 - 350^0 and for a period of time of 12 to 24 or 48 hours before averaging of the current maps is begun. Averaging is maintained until the cutoff time when the observed winds drop below the minimum wind speed or move outside the prescribed angle wedge.

Case 1: Wind from the NW

Angle wedge:	Min. wind speed:	Spinup:	Cutoff:
300^0- 350^0	**4m/s**	**12 hrs**	**24 hrs**

For this condition, represented in Figure 18, there are several events that fulfill this criterion. The events are indicated by the darkly colored wind vectors on the first plot. The conditional mean map, which is the average of the surface current response after 12 hours of the condition achievement, shows a clear current flowing toward the south at the entrance of the bay, which is intense in the northern area with speeds of about 25 cm/s. The surface current aligns generally with the wind in the offshore areas. This happens very quickly, but in the shore areas it is uncertain how the surface current responds to the wind. In the area closer to the coast, a weak cyclonic circulation is forming off Moss Landing.

Case 2- 3: Wind from the NW

Angle wedge:	Min. wind speed:	Spinup:	Cutoff:
300^0- 350^0	**4m/s**	**24 hrs**	**48- 96 hrs**

Figures 19 and 20 represent two additional case studies related to wind from the NW. In these cases, the parameters are the same as in case 1

except that the spin-up time is increased to 24 hours and the cut-off time is 48 hours or 96 hours for cases 2 and 3, respectively.. As expected, the total numbers of time events that match these criteria are less than for case 1. The numbers of darkly colored vectors on the feather plots are smaller because the conditions are more restricted. With a 24 hour same wind condition (i.e., spin-up time), the surface current out of the bay is much stronger, 30 to 35 cm/s. In the northern area, the direction is more into the bay than the previous, case-1 condition for which the spin-up time was only 12 hours.

Now, closer to the coastline in the middle of the bay, it is clear how well developed the cyclonic circulation is. The main result that is illustrated in these figures, is that when the wind blows longer, the intensity of the circulation formed in the northern area of the Bay is stronger.

Case 4-5: Wind from the NW

Angle wedge: 300^0- 350^0	Min. wind speed: 4m/s	Spinup: 48 hrs	Cutoff: 72- 96 hrs

Figures 21 and 22 depict the third condition of upwelling favorable winds. Now the spinup time is for a period of 48 hours and cutoff time is 72 hours and 96 hours for cases 4 and 5, respectively. The feather plots now show even fewer events that fulfill the prescribed conditions. The number of darkly colored vector times is smaller, but wider, because the time of the wind blowing with the condition is longer. Higher intensity of the current tends to bend more coastward in the south area of the bay. The cyclonic circulation in the middle of the Bay close to the coastline is now fully developed under these averaging conditions.

At a very long average of the HF radar data, the cyclonic circulation formed in the north area of the bay after a constant wind from the north-west is probably due to the shape of the bay and the pressure field that builds up, because of the wind forcing which moves the waters against the coast. The

geostrophic balance promotes the formation of a cyclonic gyre. It takes about 48 hours, or about 2 inertial periods to set up completely.

Case 6-7-8: Wind from the NW

Angle wedge:	Min. wind speed:	Spinup:	Cutoff:
320^0- 040^0 325^0- 045^0 330^0- 050^0	4m/s	18 hrs	72 hrs

Figures 23, 24 and 25 show three interesting cases. The wind intensity, spin up and cutoff time were not changed. However, the direction of the wind was set at three different angles wedges shifted northward by just five degrees. The differences of the surface current patterns for these situations are notorious. In the first case, for an angle-wedge between 320 and 040, the flow is toward the south and a cyclonic circulation starts forming inside the bay, although not yet well developed. For the second case, with the angle wedge between 325 and 045, the cyclonic circulation is now almost fully developed and a second circulation is observed forming out of the Bay with a strong flow in between. For the third case, the angle of the wind is between 330 and 050; two well developed gyres are shown in the surface current map. One is a cyclonic one into the Bay and another is an anticyclonic one at the entrance to the Bay. A strong current flows between these two circulations with higher intensity in the southern area of the bay. The interesting situation here is that for these conditions the surface current is more sensitive to the wind direction than to the intensity. With just a slight change in the wind direction of just 10 degrees from one scenario to another, two well developed gyre with opposite circulations were formed in a relatively small area.

b. Downwelling

Downwelling occurs with much less frequency than upwelling. That is the reason it is not possible to show what would happen when the wind blows in the same long time period for downwelling events. Most downwelling favorable

wind occurs with the wind blowing from the southeast, between 90^0 and 180^0, as shown in Figures 14 and 15. From the histogram of Figure 16 and 17, it is clear how low are the number of occurrences of these events. The stronger downwelling-favorable conditions occur mostly during winter, which makes sense because this matches the period of the fall-winter storms from late October to February.

Like the previous cases, since we want to represent the major events the angle wedge chosen was between 90^0 and 180^0 degrees, and the minimum wind intensity again was set at 4 m/s. With this angle and wind speed, the most recurring features in the HF radar current maps are shown in the following plots.

Case 1: Wind from the SE

Angle wedge:	Min. wind speed:	Spinup:	Cutoff:
90^0- 180^0	**4m/s**	**12 hrs**	**24 hrs**

The first plot of Figure 26 shows the main events developed from late October to mid-February. Ten to eleven events occurred that matched the prescribed conditions. The second plot, the conditional mean, shows that the surface currents flow toward the north at the entrance of the bay, with a stronger intensity in the south. At the coastline, the flow tends to align with it.

Case 2: Wind from the SE

Angle wedge:	Min. wind speed:	Spinup:	Cutoff:
90^0- 180^0	**4m/s**	**24 hrs**	**96 hrs**

Figure 27 represents the second condition under which the spin-up time is increased from 12 hours to 24 hours. Three main events are depicted in the feather plot, one in late December and the other two in late February. For this case, the longer spin-up time yields results that are almost the same as the previous case, but with fewer events. The only difference is the intensity of the current, which is stronger due to the longer time of the wind blowing. Again, close

to the coastline, the flow tends to go out of the Bay. The standard error depicted in the lower of the plots, for this case, is greater due to the fewer number of current maps under these prescribed conditions.

c. Other Circulations

So far cases of upwelling and downwelling have been analyzed, but this method of analysis has shown that there are other wind effects on the surface current patterns when the winds blow from other directions. There are anticyclonic circulations in the middle of the bay, strong flows out of and into the bay in the southern area close to Point Piños, and other types of circulations.

Case 1: Wind from the NE

Angle wedge:	Min. wind speed:	Spinup:	Cutoff:
000^0- 90^0	4m/s	12-24 hrs	24-48-96 hrs

Figures 28, 29, 30 and 31 represent these conditions. The first condition with a spin-up time of 12 and a cutoff of 24 hours is shown in Figure 28. The feather plot shows that this condition occurs from mid-November to late December. The second plot, conditional mean of the current maps, shows the beginning of the formation of a weak anticyclonic circulation out of the Bay. A strong circulation flows toward the west in the southern portion of the Bay off Point Piños and turns to the south after flowing out of the bay. If the cutoff now is 48 hours - the averaging starts 24 hours after the condition has been achieved - the anticyclonic circulation starts moving more into the bay and a second circulation is forming besides this one, out of the bay. The strong flow in the southern area remains the same. The next plots have the same wind speed, but now they have a spinup of 24 hours instead of 12 and with a longer period of average. It is clear the fully developed anticyclonic gyre is in the middle of the bay. For the cutoff of 96 hours, the error depicted on the third plot is less than the previous one (48 hours cutoff). For this condition, one can see how well

developed the circulation is. The stronger the wind stress for longer periods of time, the more remarkable the spin of the circulation formed in the bay is.

Case 2: Wind from the SW

Angle wedge:	Min. wind speed:	Spinup:	Cutoff:
180^0- 270^0	4m/s	12 hrs	24-60 hrs

For this case, the wind is blowing from 180^0 to 270^0 . Figures 32 and 33 represent another case that is interesting to point out. This is when the wind is blowing from the southwest, which mostly happens during the winter, but the time that the wind blows continuously from this direction is not very long. It was not possible to find periods longer that 12 hours with a wind speed of 4 m/s and up. The flow goes into the bay toward the northeast in the south area. Unfortunately the conditional standard error for this situation is quite high, so it is hard to determine what the real influence of the wind blowing from this direction on the current patterns is. This situation is associated with a cyclonic circulation out of the bay. This was also demonstrated by seeing several current maps from the HFRadarmap code named “currentviewer,” which gathers the data of the whole period. One example of one of these maps is shown in Figure 34 from August 21, 2003.

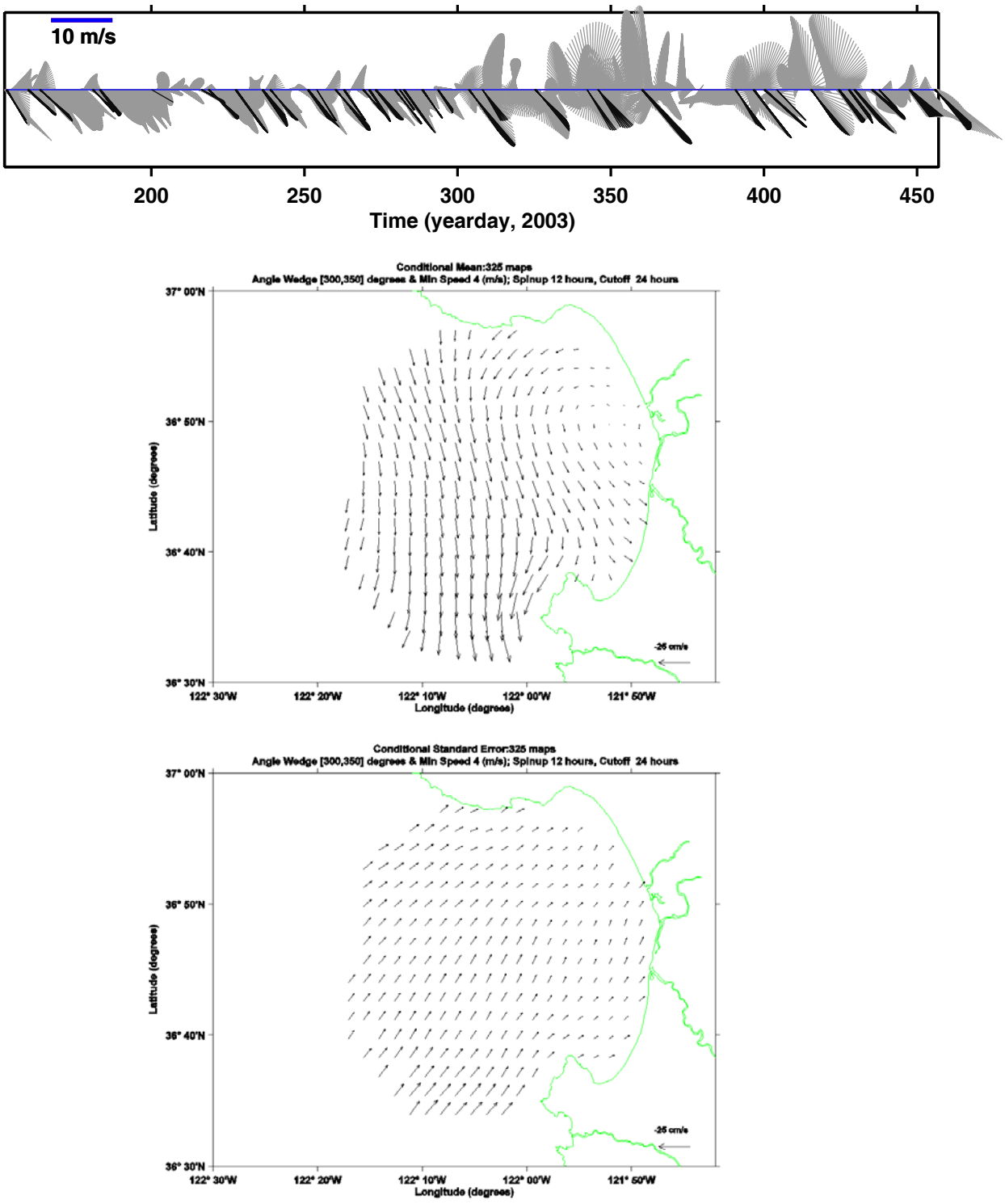

Figure 18. Wind Time Periods meeting the criteria of Speed greater than 4 m/sec, Direction between 300 and 350 degrees, Spin-up Time of 12 hours, and Cut-off Time of 24 hours (dark vectors; upper) and the Average (middle) and Standard Error (lower) of the Surface Current during these times.

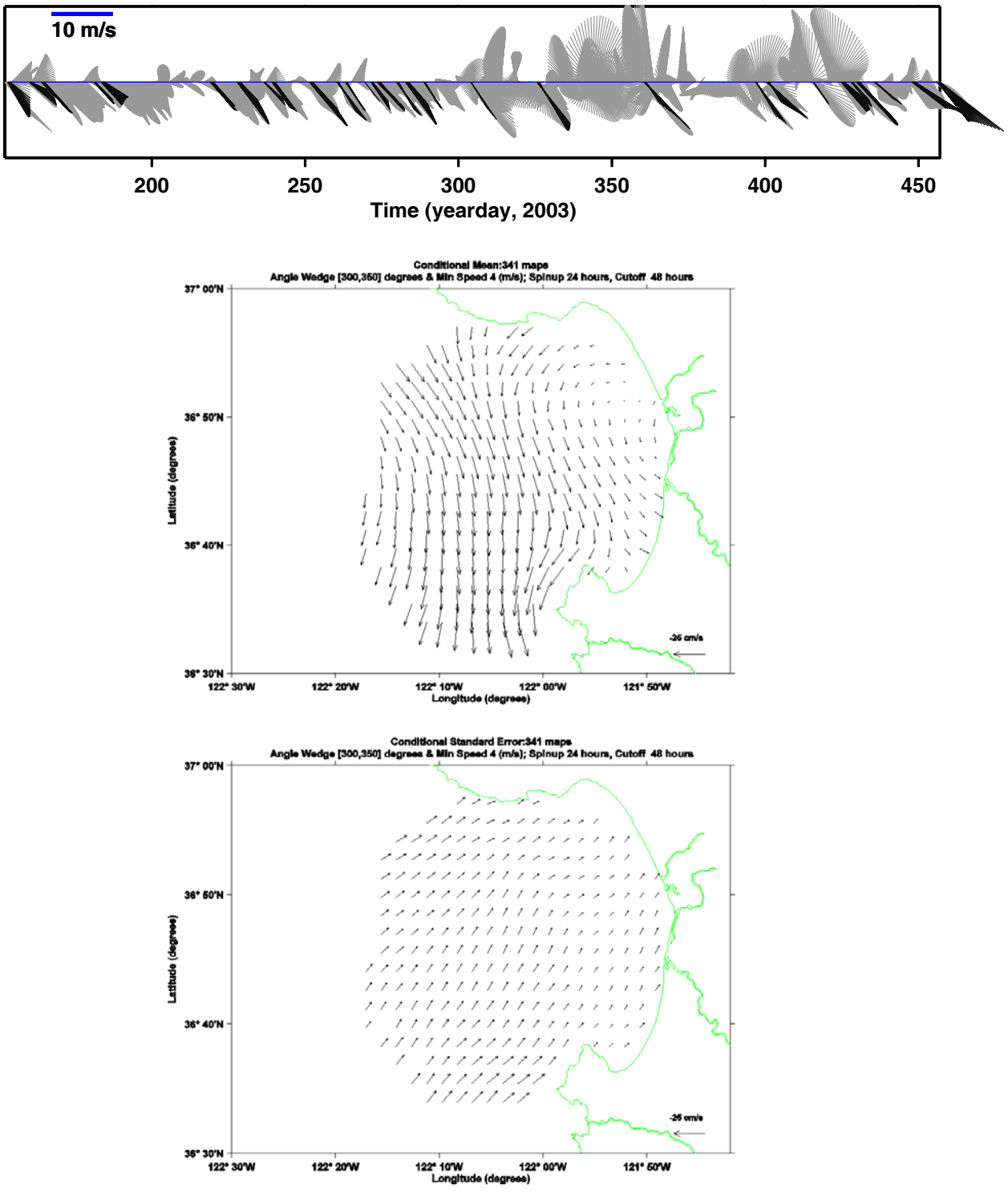

Figure 19. Wind Time Periods meeting the criteria of Speed greater than 4 m/sec, Direction between 300 and 350 degrees, Spin-up Time of 12 hours, and Cut-off Time of 48 hours (dark vectors; upper) and the Average (middle) and Standard Error (lower) of the Surface Current during these times.

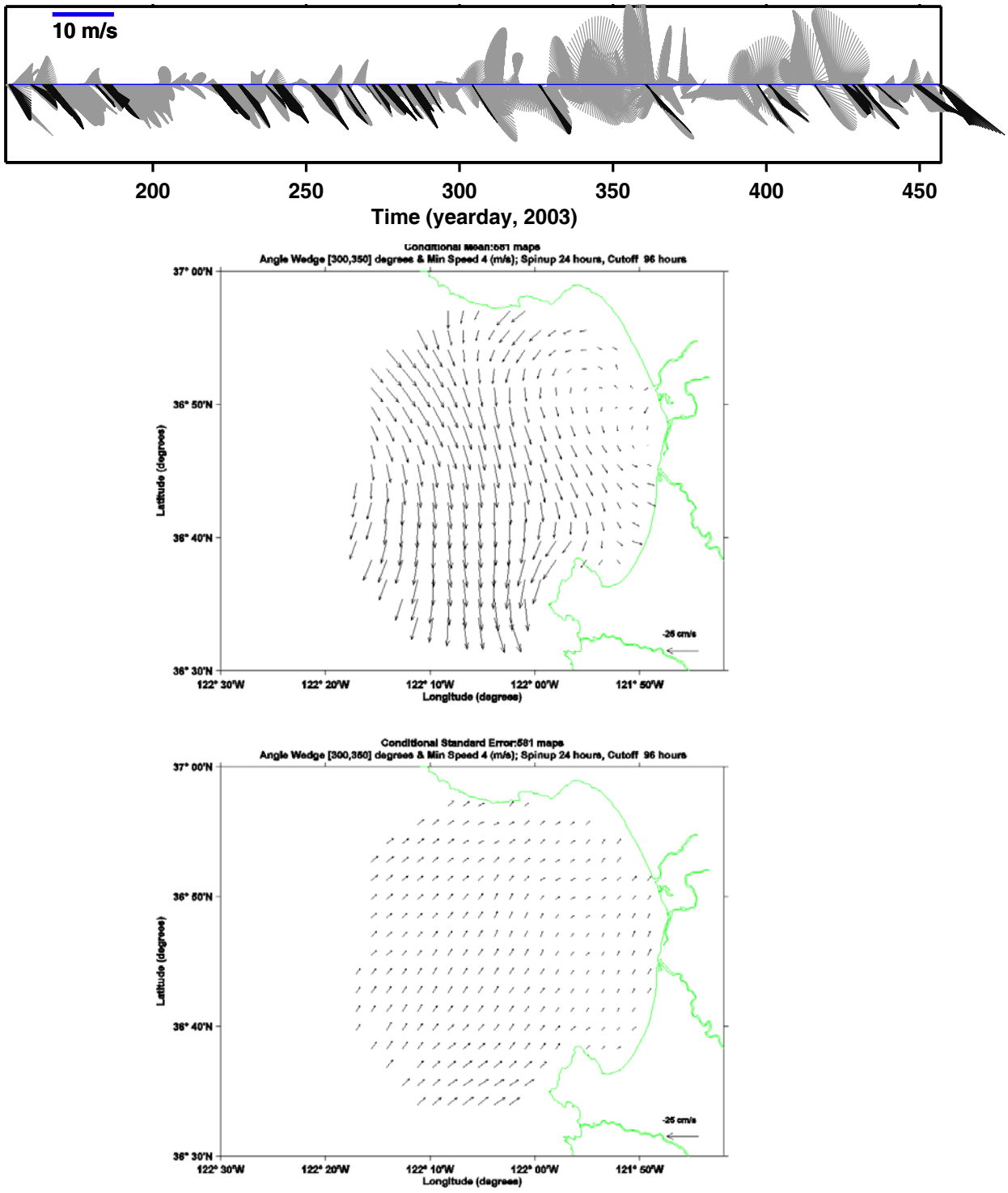

Figure 20. Wind Time Periods meeting the criteria of Speed greater than 4 m/sec, Direction between 300 and 350 degrees, Spin-up Time of 24 hours, and Cut-off Time of 96 hours (dark vectors; upper) and the Average (middle) and Standard Error (lower) of the Surface Current during these times.

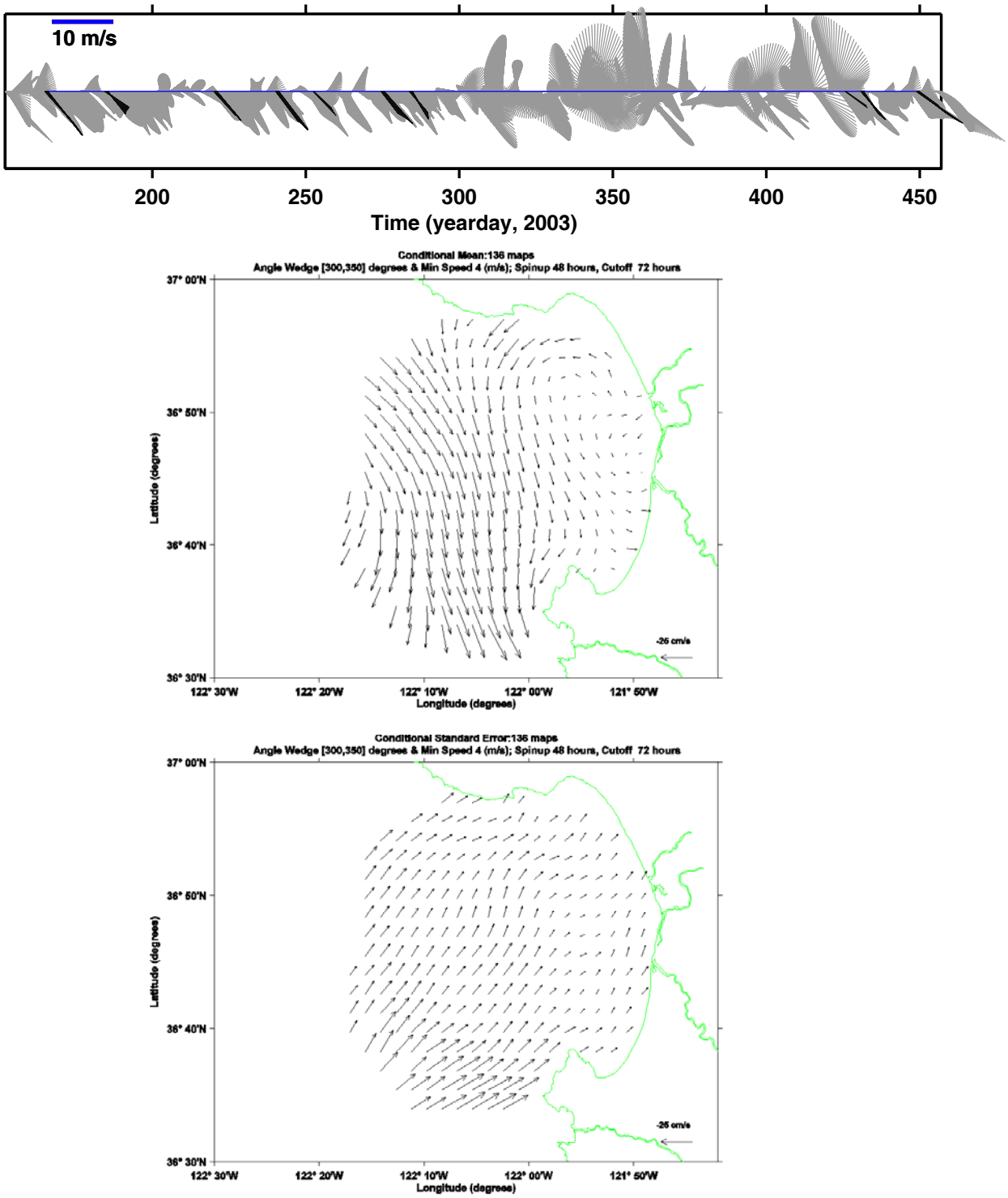

Figure 21. Wind Time Periods meeting the criteria of Speed greater than 4 m/sec, Direction between 300 and 350 degrees, Spin-up Time of 48 hours, and Cut-off Time of 72 hours (dark vectors; upper) and the Average (middle) and Standard Error (lower) of the Surface Current during these times.

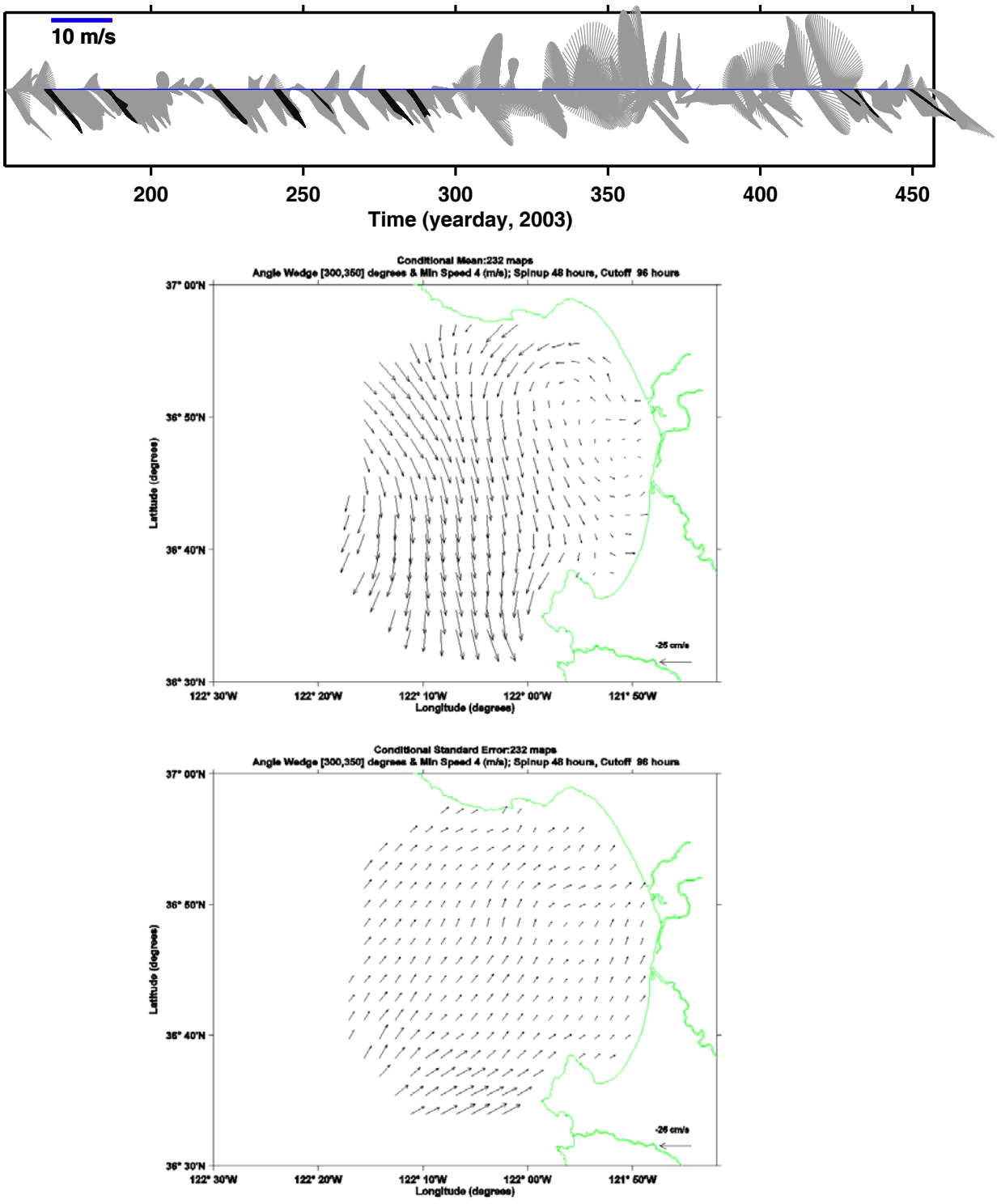

Figure 22. Wind Time Periods meeting the criteria of Speed greater than 4 m/sec, Direction between 300 and 350 degrees, Spin-up Time of 48 hours, and Cut-off Time of 96 hours (dark vectors; upper) and the Average (middle) and Standard Error (lower) of the Surface Current during these times.

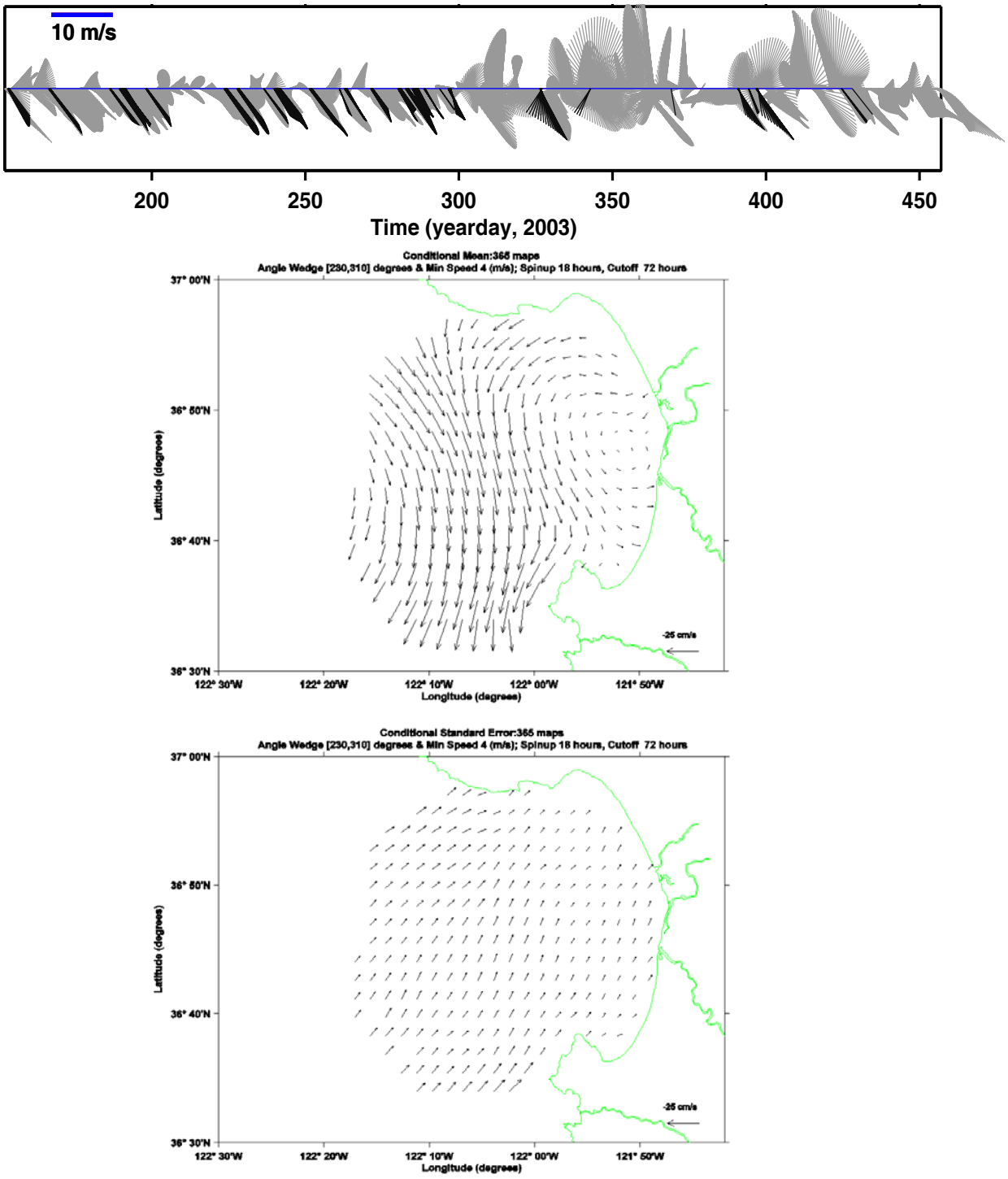

Figure 23. Wind Time Periods meeting the criteria of Speed greater than 4 m/sec, Direction between 320 and 040 degrees, Spin-up Time of 18 hours, and Cut-off Time of 72 hours (dark vectors; upper) and the Average (middle) and Standard Error (lower) of the Surface Current during these times.

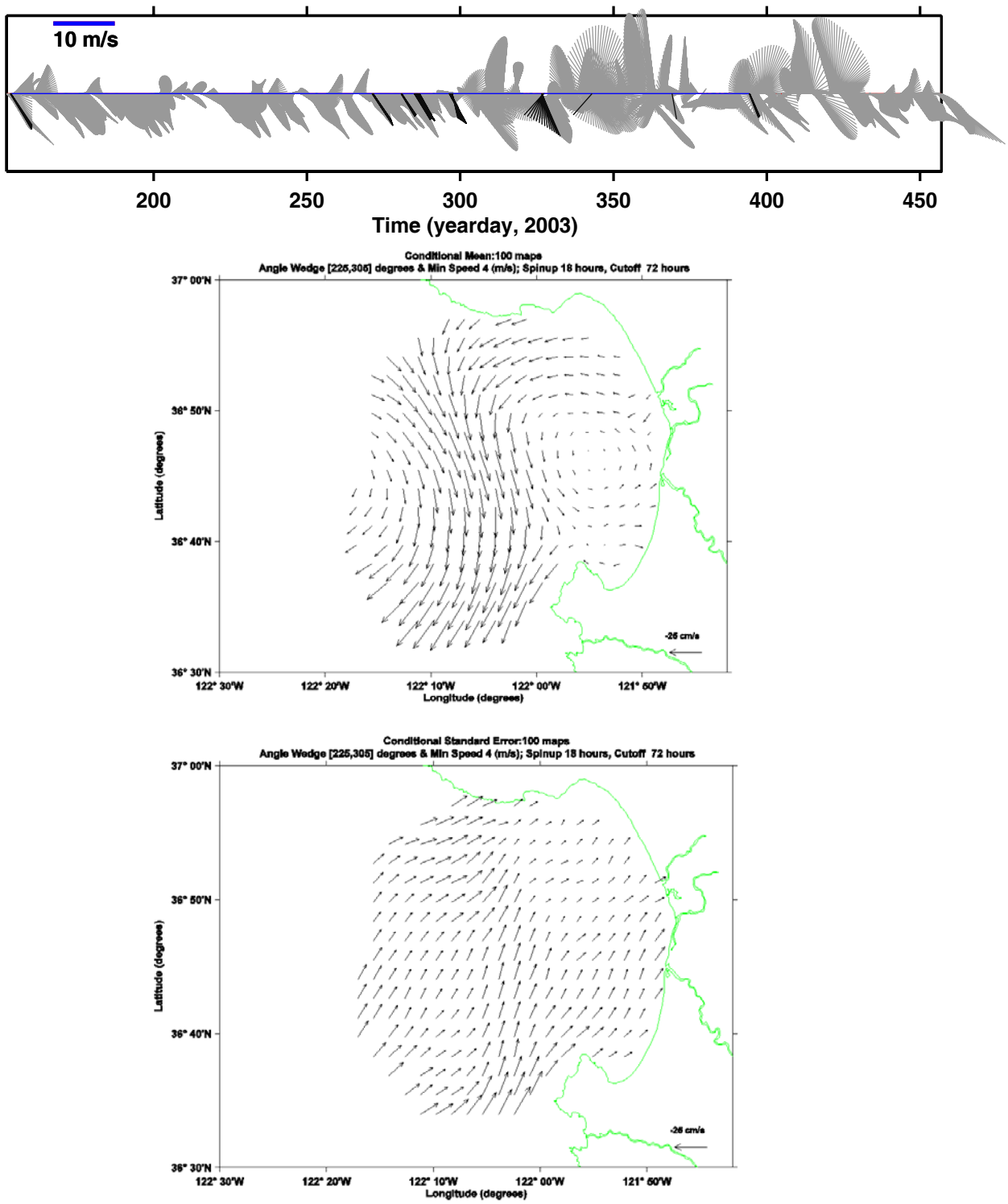

Figure 24. Wind Time Periods meeting the criteria of Speed greater than 4 m/sec, Direction between 325 and 045 degrees, Spin-up Time of 18 hours, and Cut-off Time of 72 hours (dark vectors; upper) and the Average (middle) and Standard Error (lower) of the Surface Current during these times.

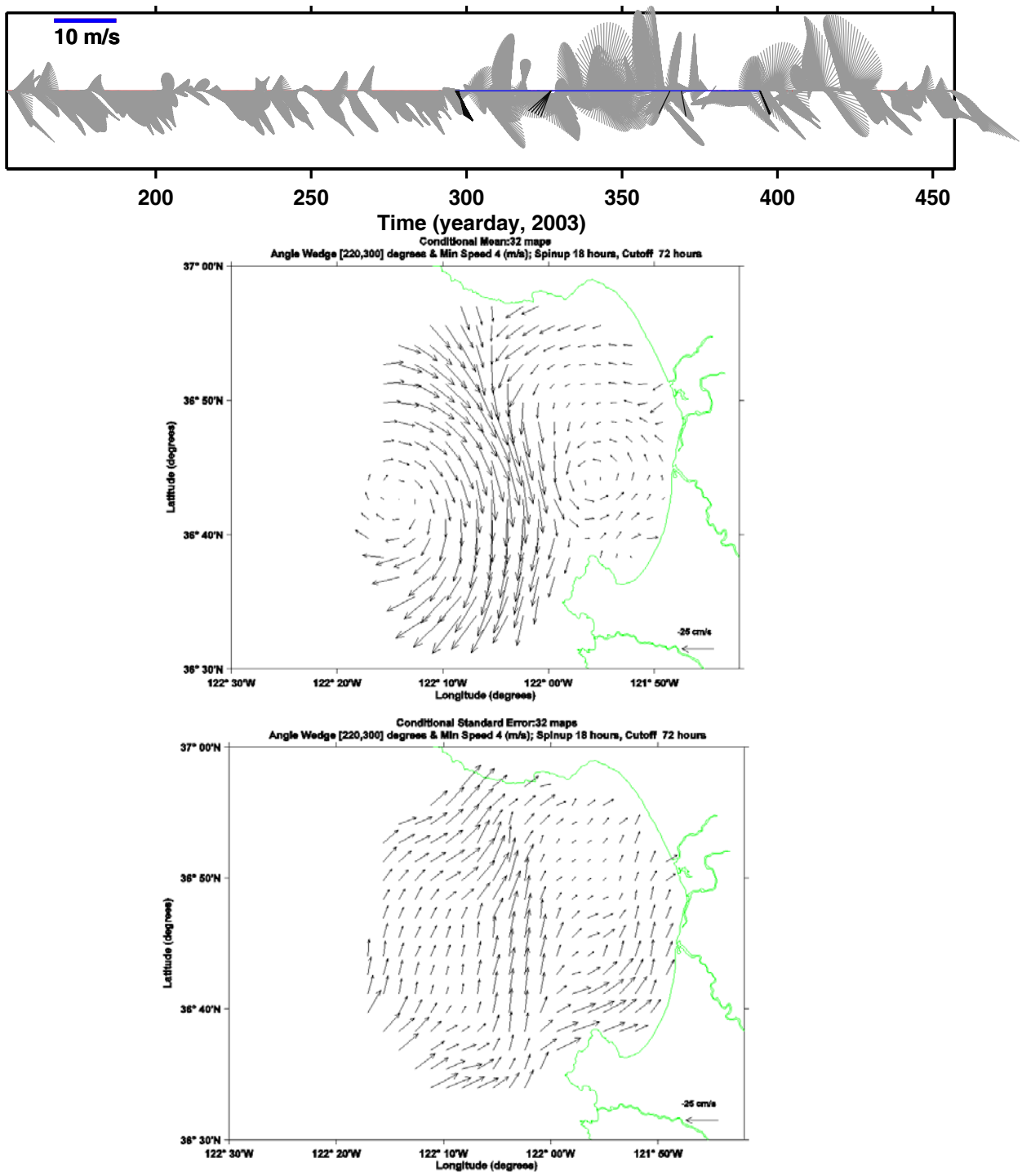

Figure 25. Wind Time Periods meeting the criteria of Speed greater than 4 m/sec, Direction between 330 and 050 degrees, Spin-up Time of 18 hours, and Cut-off Time of 72 hours (dark vectors; upper) and the Average (middle) and Standard Error (lower) of the Surface Current during these times.

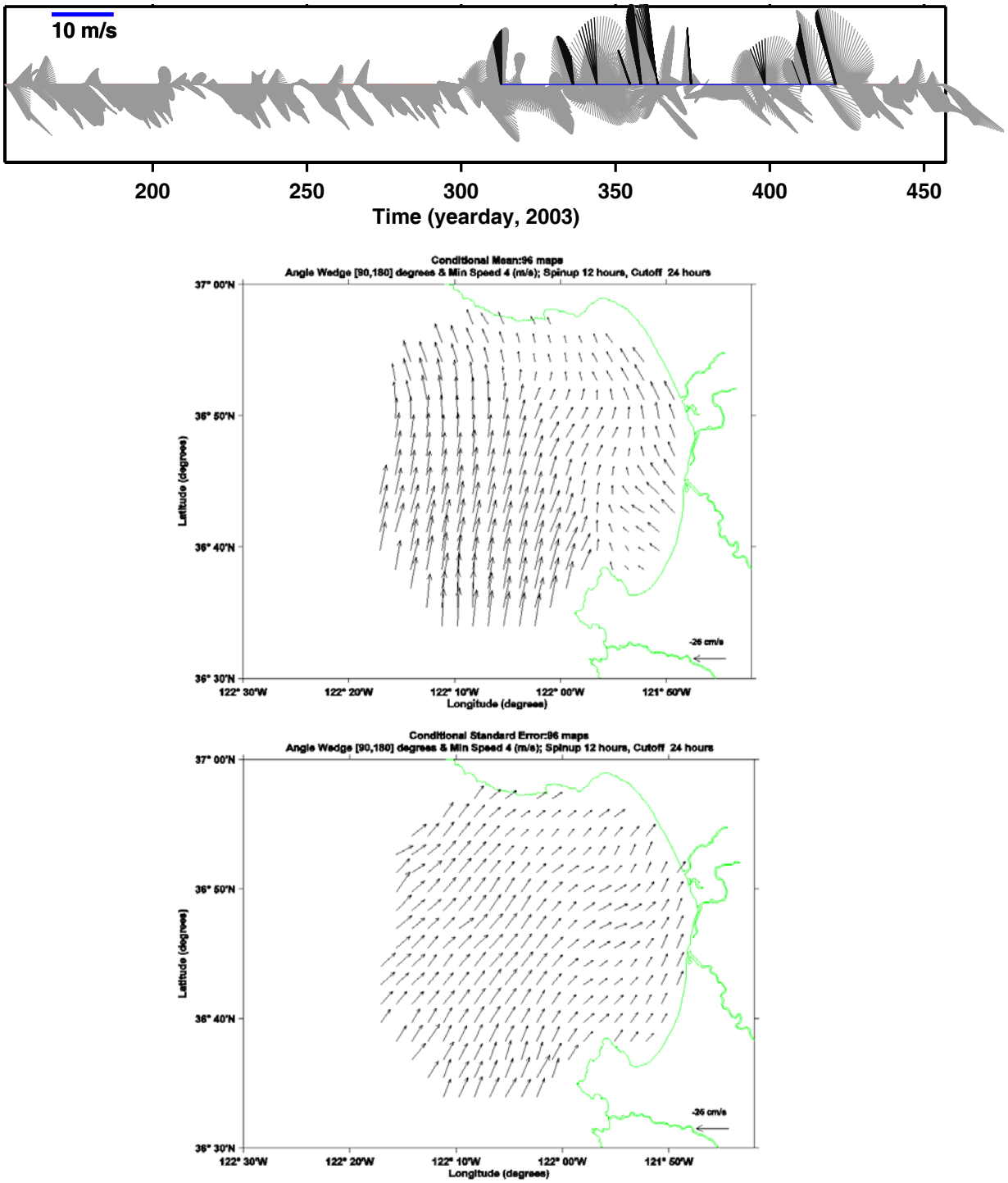

Figure 26. Wind Time Periods meeting the criteria of Speed greater than 4 m/sec, Direction between 90 and 180 degrees, Spin-up Time of 12 hours, and Cut-off Time of 24 hours (dark vectors; upper) and the Average (middle) and Standard Error (lower) of the Surface Current during these times.

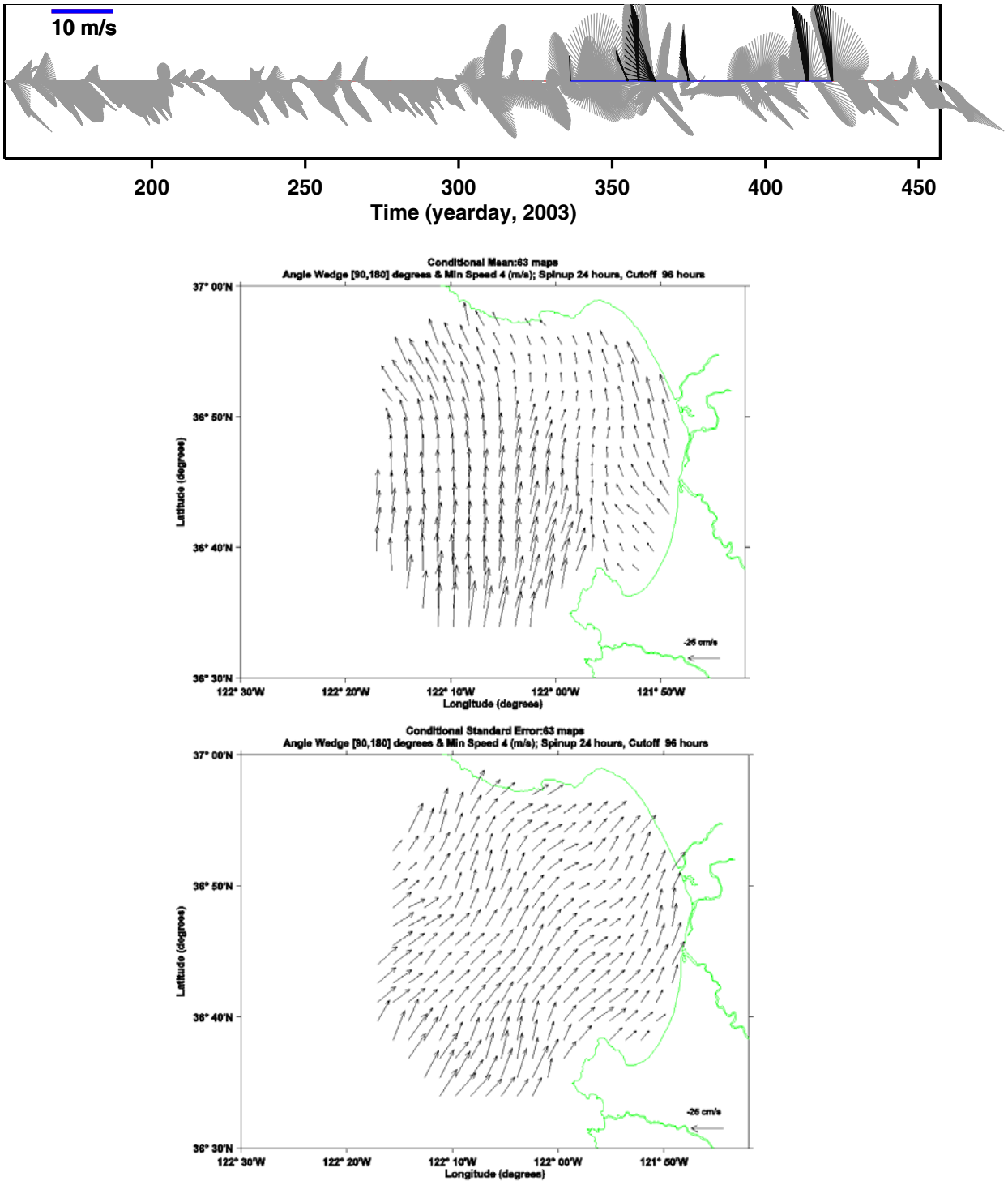

Figure 27. Wind Time Periods meeting the criteria of Speed greater than 4 m/sec, Direction between 90 and 180 degrees, Spin-up Time of 24 hours, and Cut-off Time of 96 hours (dark vectors; upper) and the Average (middle) and Standard Error (lower) of the Surface Current during these times.

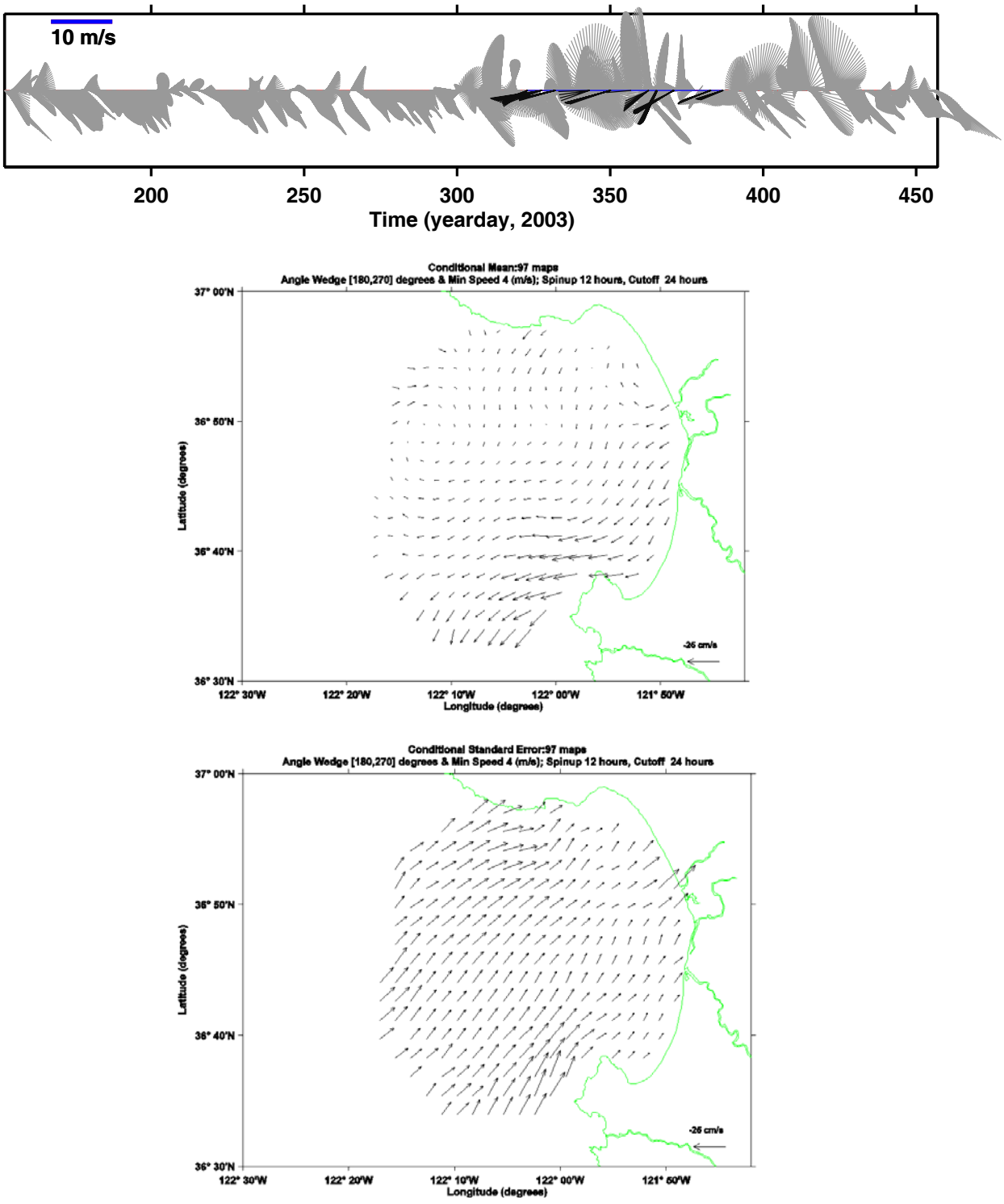

Figure 28. Wind Time Periods meeting the criteria of Speed greater than 4 m/sec, Direction between 000 and 90 degrees, Spin-up Time of 12 hours, and Cut-off Time of 24 hours (dark vectors; upper) and the Average (middle) and Standard Error (lower) of the Surface Current during these times.

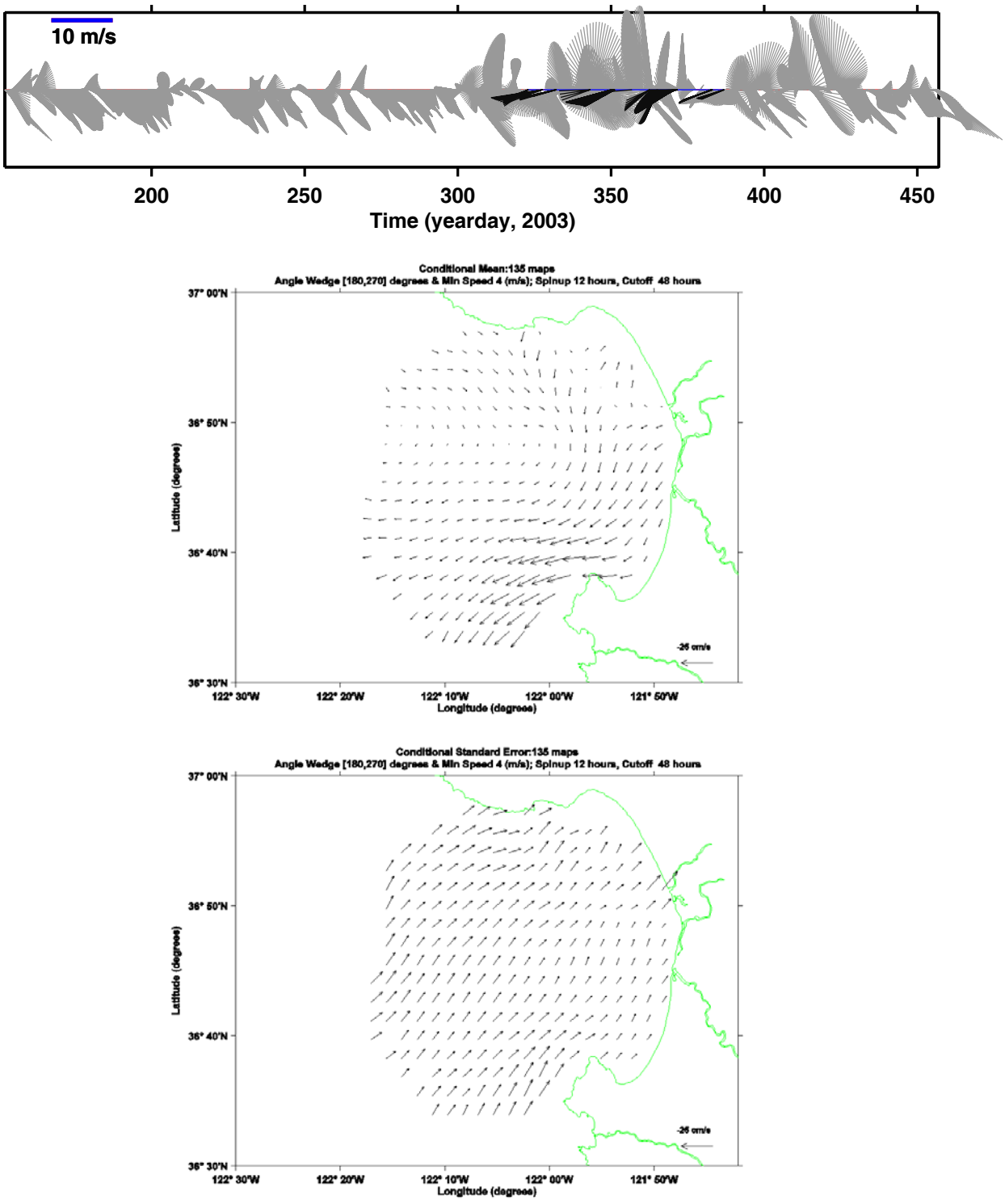

Figure 29. Wind Time Periods meeting the criteria of Speed greater than 4 m/sec, Direction between 000 and 90 degrees, Spin-up Time of 12 hours, and Cut-off Time of 48 hours (dark vectors; upper) and the Average (middle) and Standard Error (lower) of the Surface Current during these times.

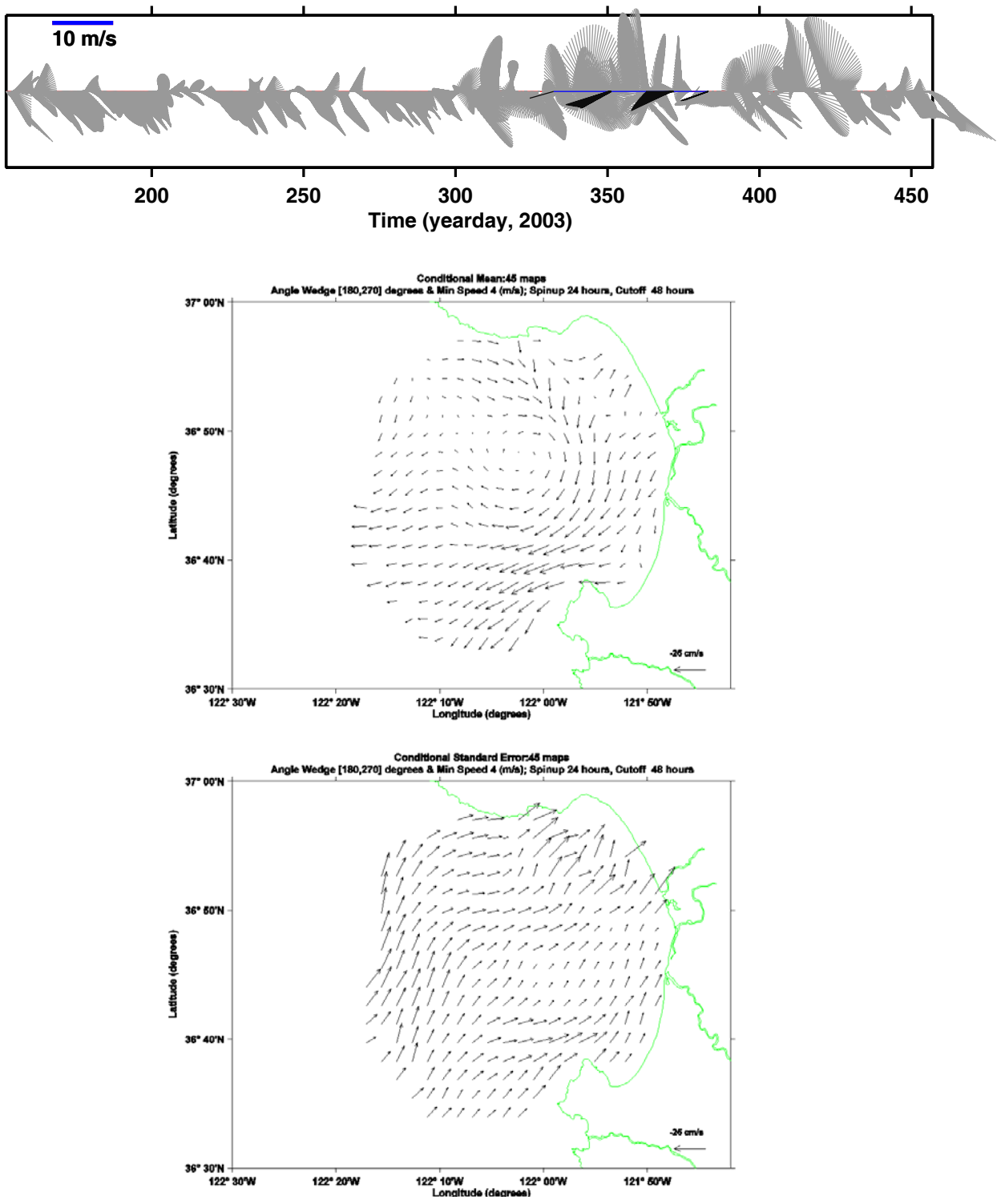

Figure 30. Wind Time Periods meeting the criteria of Speed greater than 4 m/sec, Direction between 000 and 90 degrees, Spin-up Time of 24 hours, and Cut-off Time of 48 hours (dark vectors; upper) and the Average (middle) and Standard Error (lower) of the Surface Current during these times.

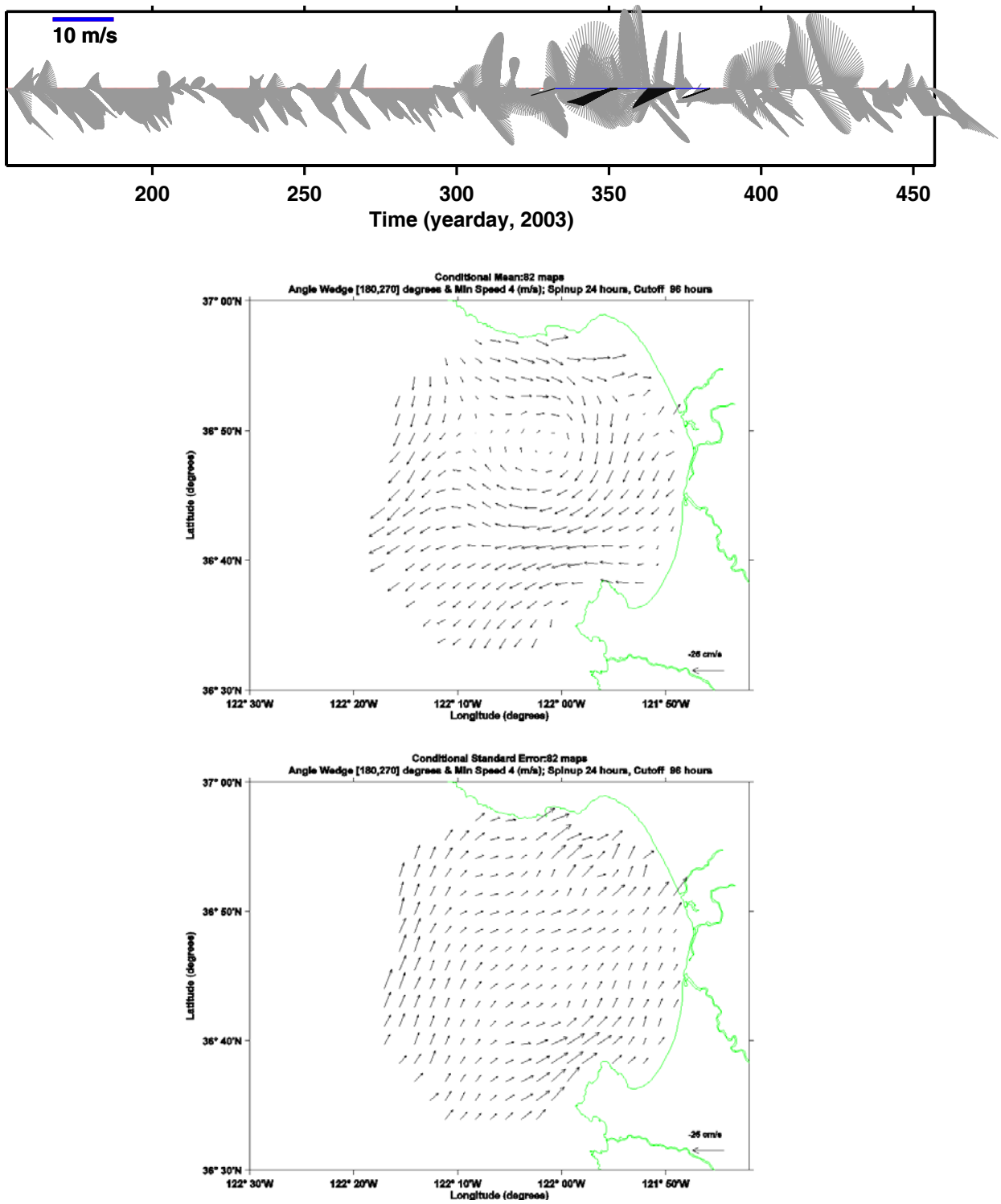

Figure 31. Wind Time Periods meeting the criteria of Speed greater than 4 m/sec, Direction between 000 and 90 degrees, Spin-up Time of 24 hours, and Cut-off Time of 96 hours (dark vectors; upper) and the Average (middle) and Standard Error (lower) of the Surface Current during these times.

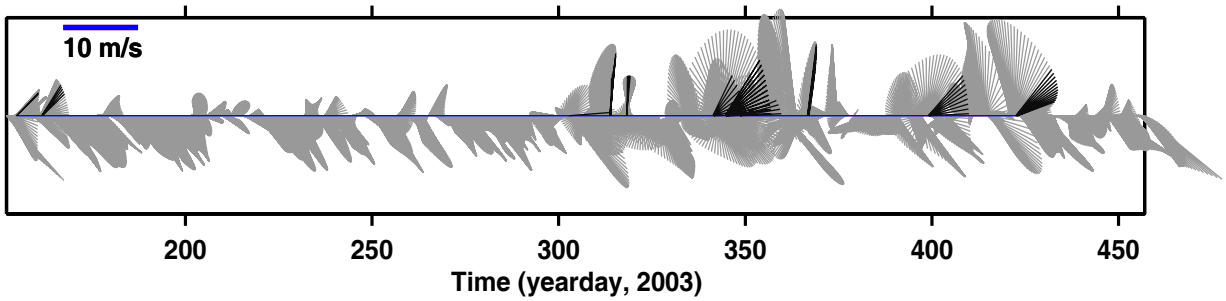

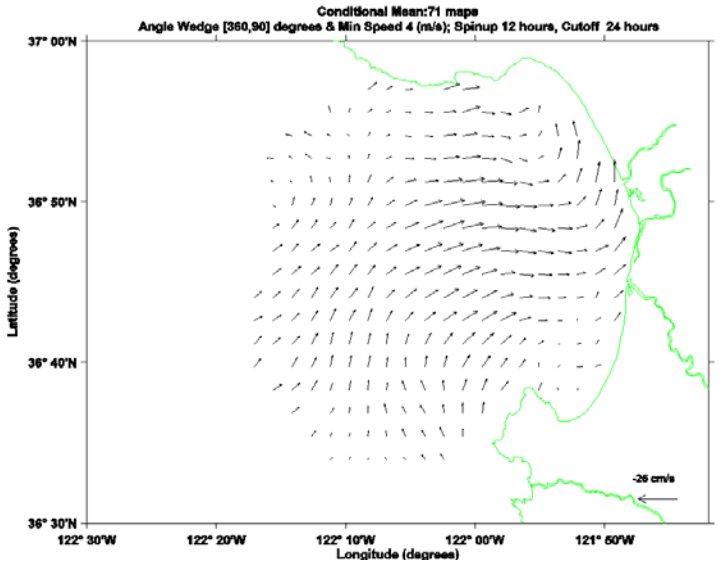

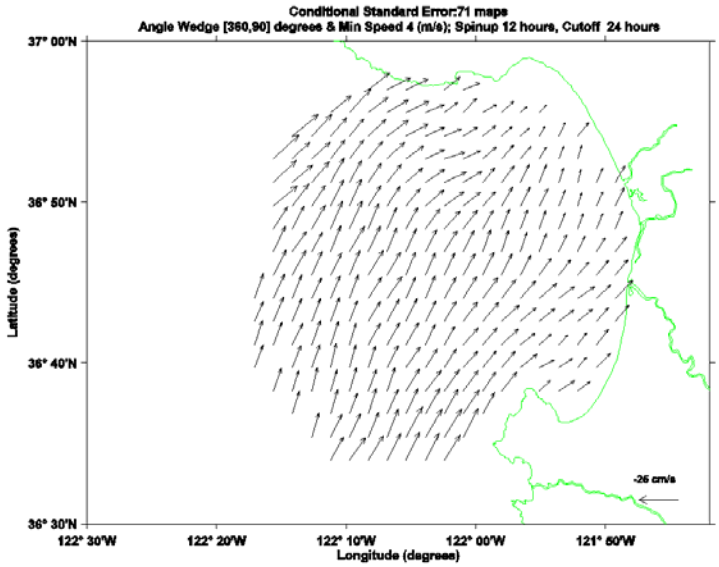

Figure 32. Wind Time Periods meeting the criteria of Speed greater than 4 m/sec, Direction between 180 and 270 degrees, Spin-up Time of 12 hours, and Cut-off Time of 24 hours (dark vectors; upper) and the Average (middle) and Standard Error (lower) of the Surface Current during these times.

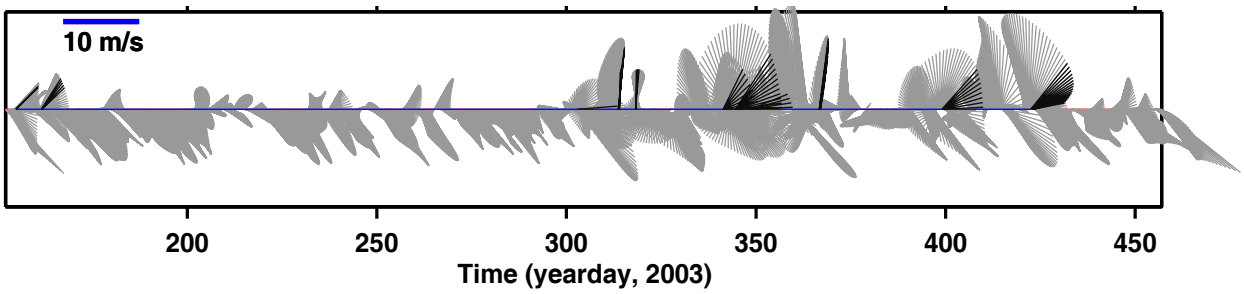

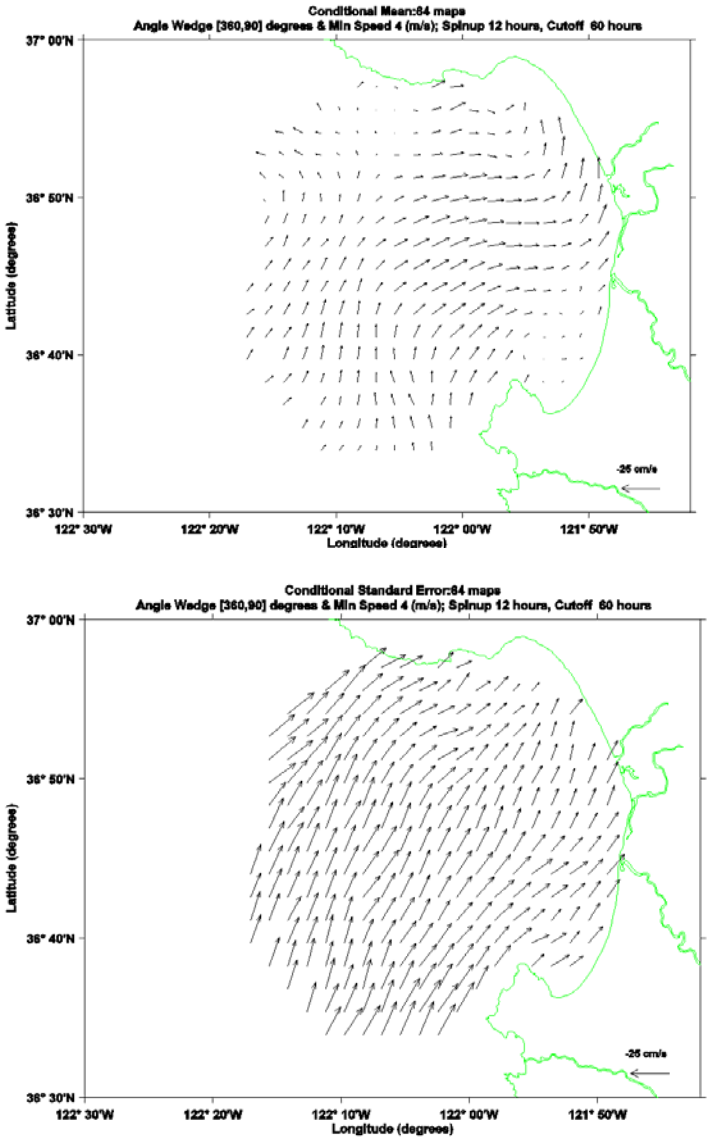

Figure 33. Wind Time Periods meeting the criteria of Speed greater than 4 m/sec, Direction between 180 and 270 degrees, Spin-up Time of 12 hours, and Cut-off Time of 60 hours (dark vectors; upper) and the Average (middle) and Standard Error (lower) of the Surface Current during these times.

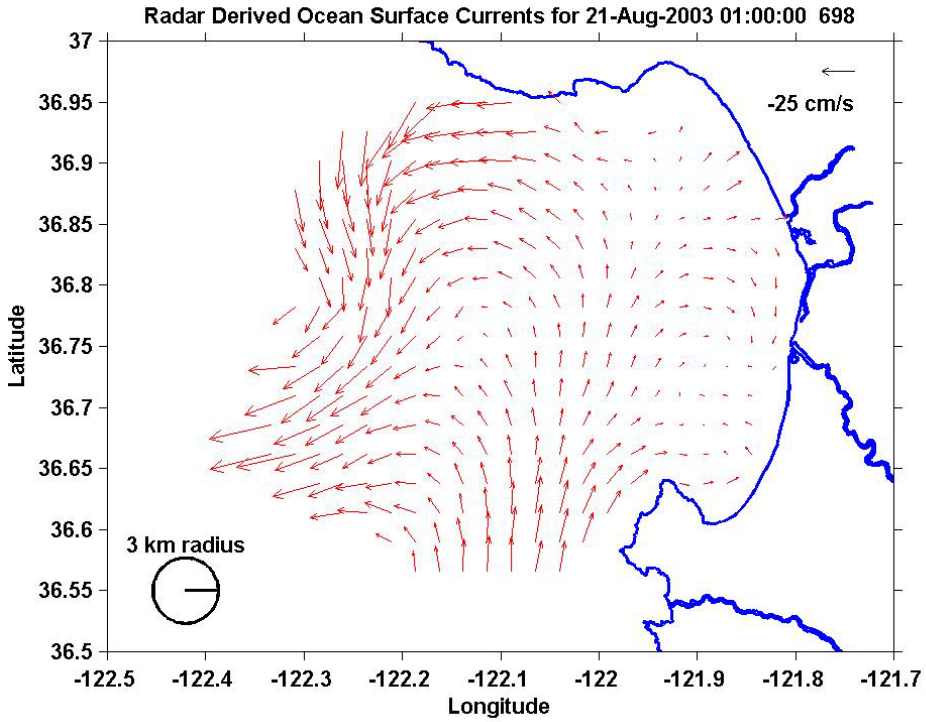

Figure 34. HF Current map of August 21, 2003.

3. Bottom-Fixed ADCP and HF Radar Grids

One of the interesting unknown details about the Monterey Bay surface current circulation is the current patterns very close to the shore and how they relate to the larger-scale patterns observed in the HF radar-derived current maps. For this reason, an investigation of current observations very close to the coastline taken by the PISCO program was incorporated into this study. Two sites were selected: Hopkins and Terrace point, in the south and in the north area of the Bay, respectively. To be able to predict when or why the circulation is in or out of the Bay for the coastal areas nearby Hopkins and Terrace Point was the goal of the following analysis. Sometimes the circulation is clockwise and at other times it reverses without following obvious changes in wind forcing.

A more specific question that can be addressed with the available data sets is the question of how far offshore is the current measured by bottom-fixed ADCP from the Hopkins site or the Terrace Point site coherent? The existence of

the HF radar-derived surface current maps provides the possibility to answer this question. Difficulties result when one tries to compare the HF radar-derived currents 2-3 km from shore with the currents observed very close (less than 1 km) to shore at the Hopkins or Terrace Point locations. Rather than assume a one-to-one correspondence between the offshore currents and the near-coastal currents, the HF radar data were used to relate the pattern information in the large-scale flow field to the events observed at the coastal sites. For example, different HF grid points were selected quite far away from the Hopkins ADCP in order to describe the sense of flow in that area. Before describing the results, it is necessary to point out how the current components from the different HF radar grid points were selected.

a. HF Grid Point information

There are a total of 328 HF radar total vector grid points within the Bay formed by the overlapping of radial current observations from the five antennas. Following the total vector mapping step, *u* and *v* components can be extracted independently for each one of these grid points. Figure 35 shows the location of six different HF grid points chosen between the M1 Buoy and the Hopkins coastal site. Figure 36 depicts the *u* and *v* component of all six grid points. This was done to see how well correlated *u* and *v* components are between the different grid points close together. The plot in these figures show the differences in the intensity of the current with higher values for the negative components. The *v* component is stronger than *u*, and it has the maximum strength between Julian days 230 and 235 (this is from August 18 to August 24), one or two days after the end of one of the main upwelling periods. The grid point located more to the west, indicates stronger *u* and *v* velocity than the grid points located to the east or more into the bay. The current maps have shown previously that the strongest speed intensity is at the entrance of the bay in the southern area. Despite the variations in magnitude, the events are highly correlated across all six HF radar grid points shown in the figures.

Figures 37 and 38 show the direction and intensity information from the HF radar grid points as vector feather plots. From these feather plots, it is clear how the current intensity decays from west to east, with maximum magnitudes at the first HF radar grid point outside the entrance to the bay.

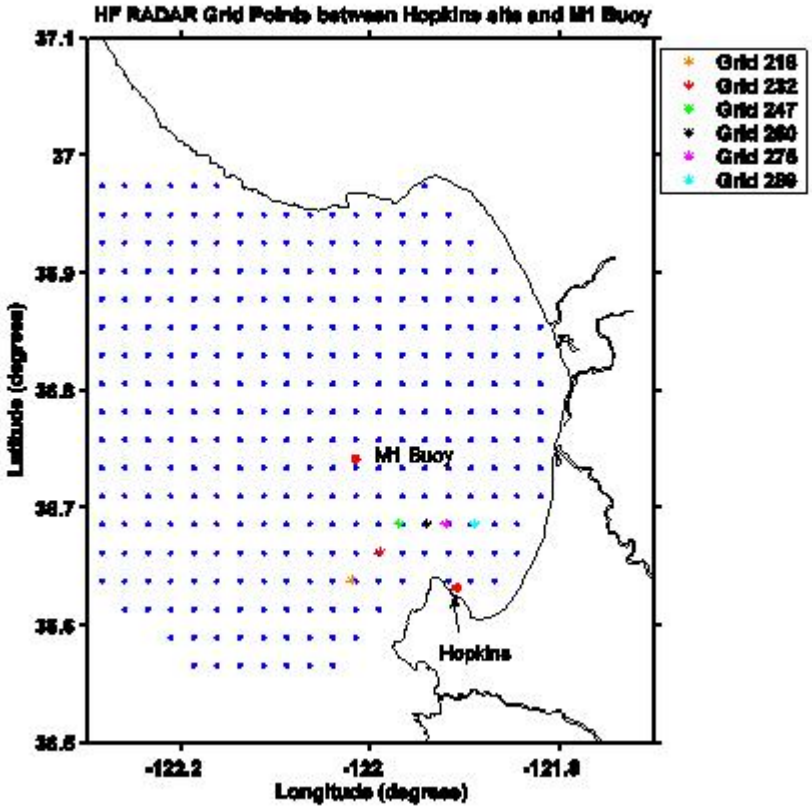

Figure 35. Identification of the Grid Points between M1 Buoy and Hopkins Site.

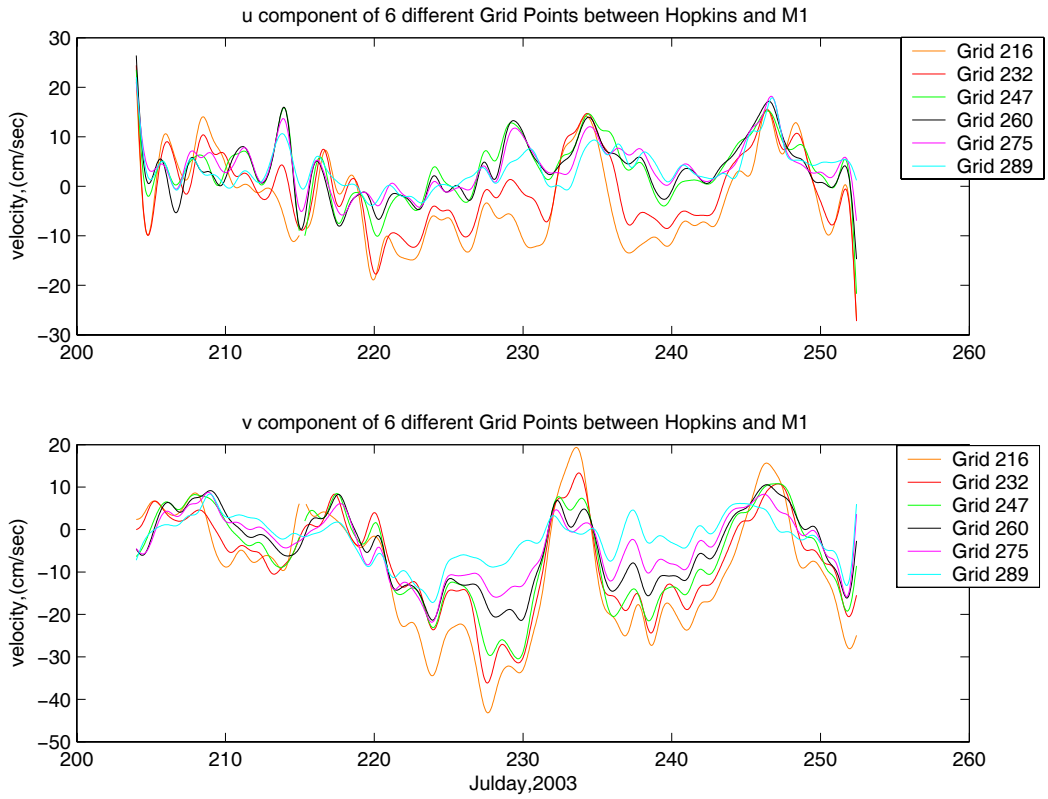

Figure 36. U component of six different HF grid points between M1 Buoy and Hopkins site.

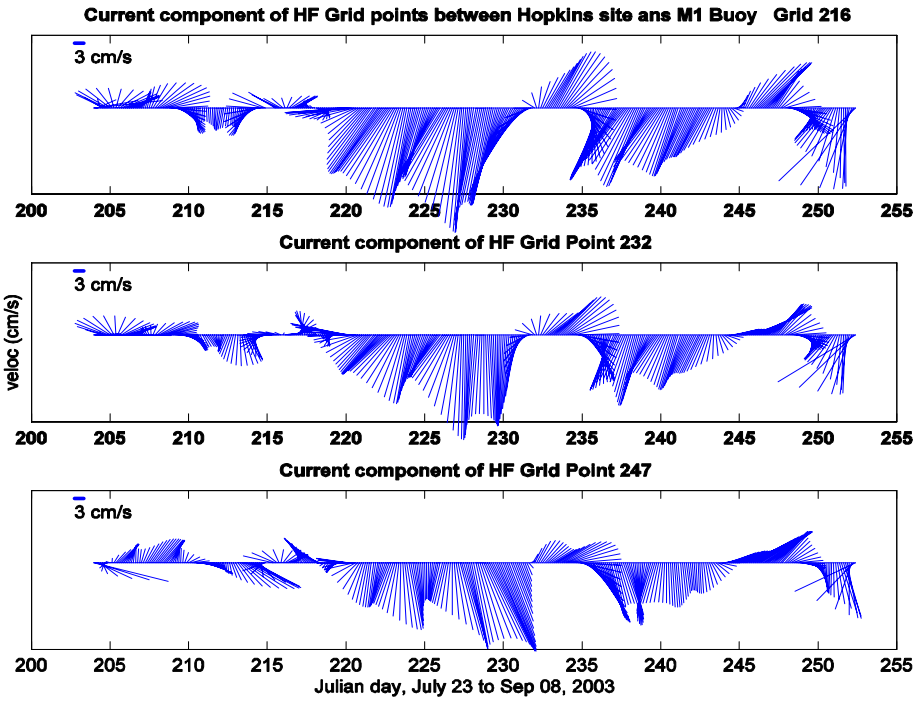

Figure 37. Feather plot of surface current of HF grid points 260,275,289.

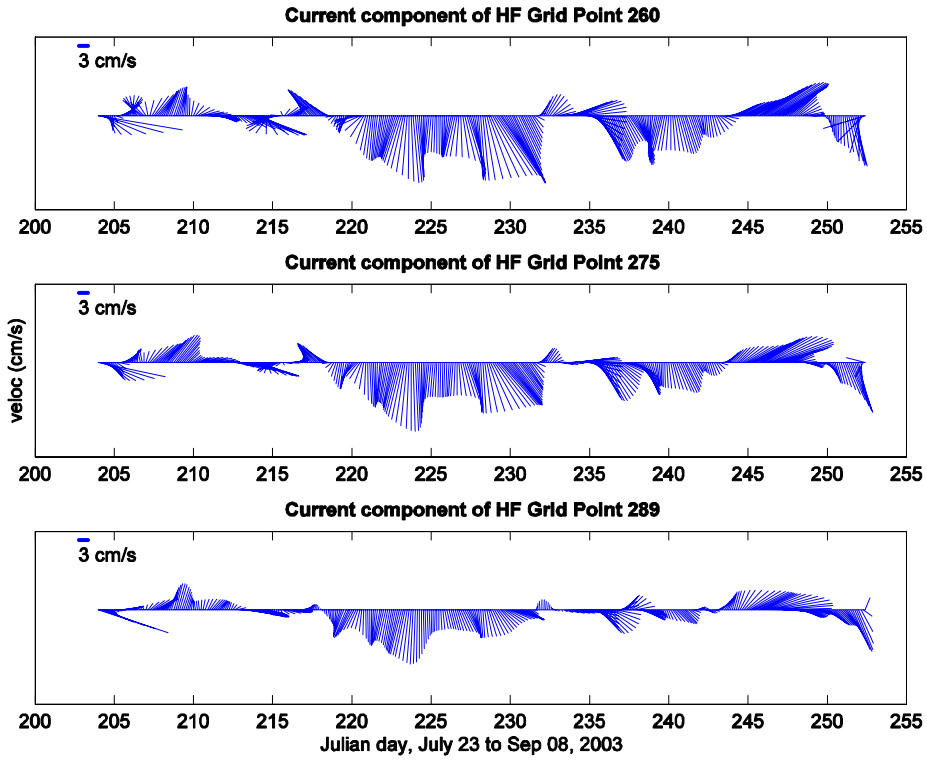

Figure 38. Feather plot of surface current of HF grid points 216,232, 247.

b. Bottom-Fixed ADCP

The data from two bottom-fixed ADCP were used for the present study. Data from a third location, Sandhill Bluff, was discarded because it is located too far away from the entrance of the bay and is not very useful for the analysis. Data from the Hopkins site and Terrace Point were analyzed. The data from these sites were also filtered with the same low-pass filter used for the HF radar-derived surface current maps.

Figures 39 and 40 show the position of both bottom-fixed ADCPs and the corresponding closest HF radar grid points. For comparison purposes, the first panels of Figures 41 and 42 show the intensity and direction of the current in a feather plot for Terrace Point and Hopkins sites, respectively. Because of the location of it these instruments, very close to the shore with an average depth of just 20 m, it is difficult to accurately estimate the surface current a short distance from these sites. However, the direction of the surface current which is consistent with the coastline for each of the two sites, can be estimated.

From the first plot of Figure 41, Terrace Point, it is clear how the surface current aligns to the coastline. According to this plot, most of the flow is out of the bay, but from the second plot of the same figure, the current from the HF radar grid points have almost equal negative and positive components. The intensity is also different. The data from the HF grid point is stronger than the one from the ADCP; however four major peaks are coincidental for both. These are between yeardays 210 and 215, 218 and 220, 225 and 230 and 237 and 240. Grid points 178 and 195 correlate better to the ADCP data, which makes sense since both are the closest ones to the instrument position.

At both near-coastal ADCP locations the current directions are observed to be nearly rectilinear with flow moving in one of two directions parallel to the coastline. Clearly the flow at those locations is not free to move in any direction. However, the velocity records each contain obvious events for which the near-coastal flow reverses or changes its magnitude significantly. These events can be expected to also be present in the offshore HF radar-derived

current patterns, although not necessarily in an obvious way. One way to highlight the events in the near-coastal ADCP data is to rotate the vector currents into the alongshore direction and then to extract the scalar alongshore component for comparisons with various velocity components from the HF radar grid. For the data from the Hopkins site, this was done by rotating the current vector by 40 degrees.

The results shown in Figure 41 suggest that the alongshore flow at the Terrace Point site is well correlated with the east-west flow just offshore at several of the HF radar grid points. The HF radar data, however, indicate changes in sign of the east-west flow at some locations during some events. This is explained below using observations of the larger-scale surface current patterns from the entire HF radar grid.

The results shown in Figure 42 attempt to relate the near-coastal observations at the Hopkins site to the offshore surface currents at several HF radar grid points. The rotated alongshore current components from the Hopkins site ADCP data are presented in the third panel of Figure 42 along with the east-west components from several nearby HF radar grid locations. From the feather plot of Figure 42, three major events can be identified. The first is around yearday 215. The second one is yearday 233 and the third one yearday 245. If we compare these events with the wind record of Figure 10 showing the details of the wind direction and intensity during August and September, those periods corresponds to periods of relaxation. The latest two events coincides with the end of two upwelling events. So it is likely that these two peaks in the ADCP record represent the near-coastal response to these 2 events. However since the first one of the peaks at yearday 215 does not coincide with any major event, it is hard to make any connection between the wind stress and the current pattern close to Hopkins point. From the time series plots, however, it can be seen that the near-coastal flow component is in the opposite direction compared with the flow at the HF radar grid points in terms of whether the flow is entering or leaving Monterey Bay. This can be explained by assuming that the flow goes into the bay near the chosen radar grid points and out of the bay close to Hopkins. As

a result, it can be inferred that during the major event periods a small clockwise circulation cell forms in the southern part of the bay.

Figure 43 depicts two surface current maps from the HF radar network that help to interpret the results of the time series comparisons with the near-coastal ADCP observations. With regard to the Terrace Point location at the northern end of the bay, it is seen to be near a convergence point along the coastline for which flow is often leaving the bay to the east of Terrace Point and entering the bay to the west of Terrace Point with the flow ultimately joining the strong southward current that forms across the mouth of the bay under upwelling-favorable wind conditions. Hence, the single-point measurement at Terrace Point does contain information about the larger-scale circulation in the region, but it would be difficult to extract that information with only the ADCP time series.

With regard to the Hopkins location, the two surface current pattern examples in Figure 43 show that the near-coastal flow at that site can be both in phase with the offshore currents under some upwelling conditions or it can be in the opposite direction as the flow a few kilometers offshore due to the presence of a small anticyclonic circulation cell in the southern portion of Monterey Bay. In this case, the time series presented in Figure 42 suggest that the out-of-phase, circulation cell configuration is the more commonly occurring situation for southern Monterey Bay.

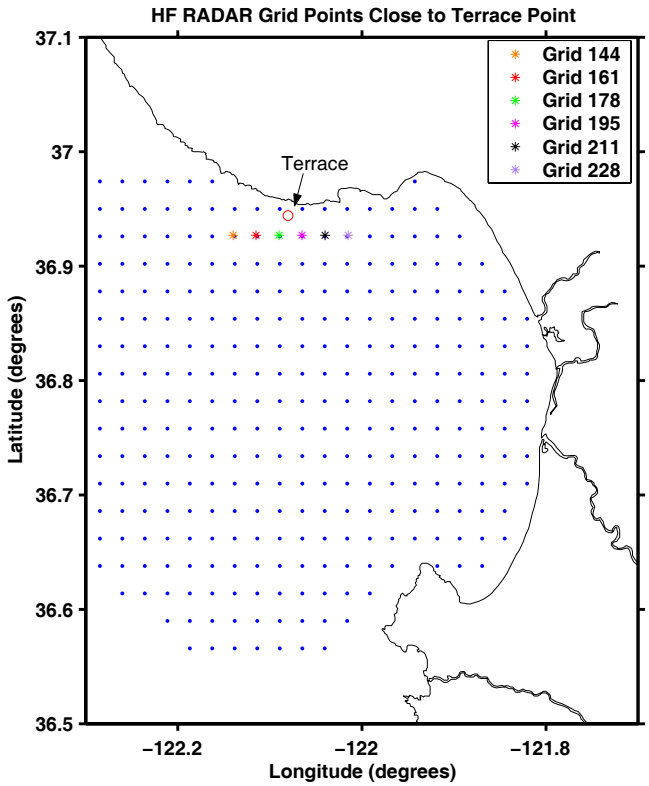

Figure 39. Location of HF grid points below Terrace Point.

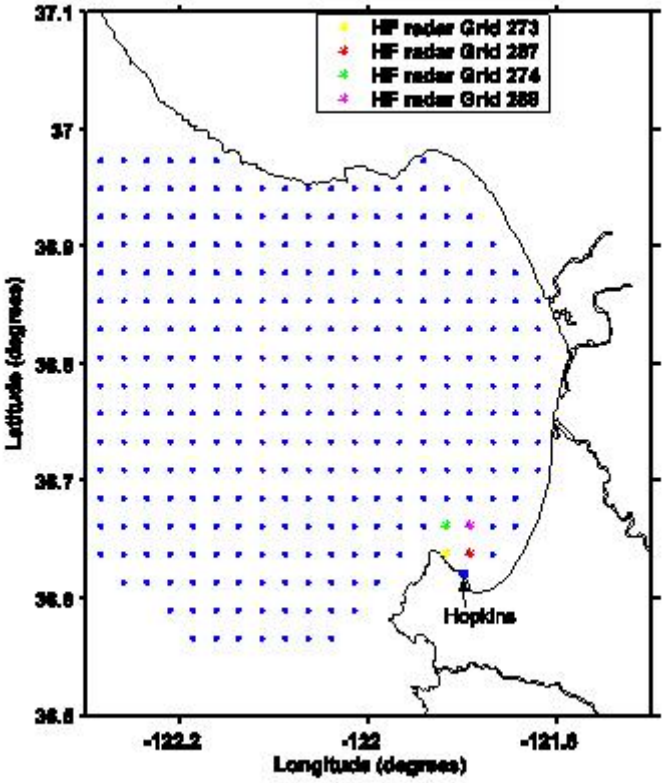

Figure 40. Location of HF grid points close to Hopkins.

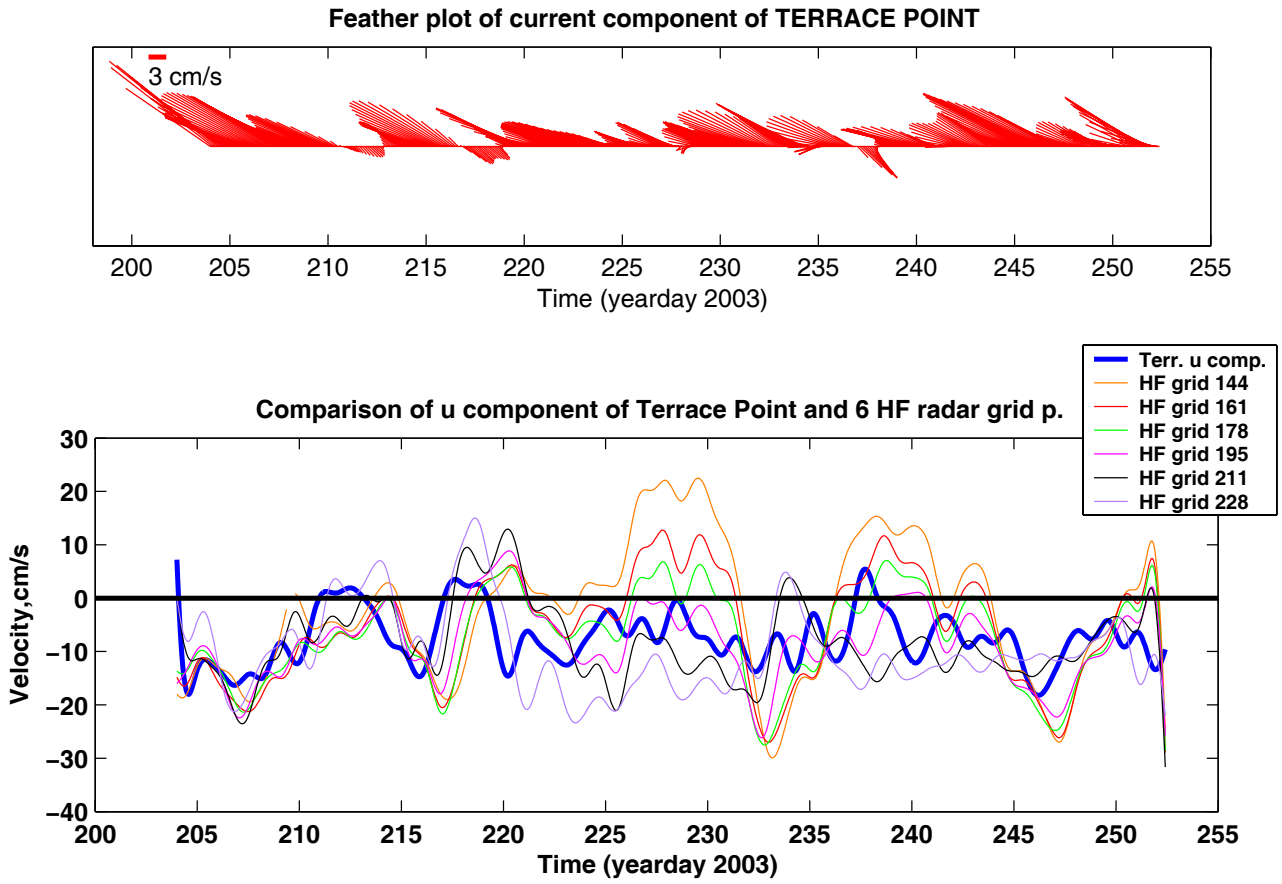

Figure 41. **First plot depicts intensity and direction of u component at Terrace Point. Second one, shows the comparison of u component of Terrace Point and the different u components from the HF grid points.**

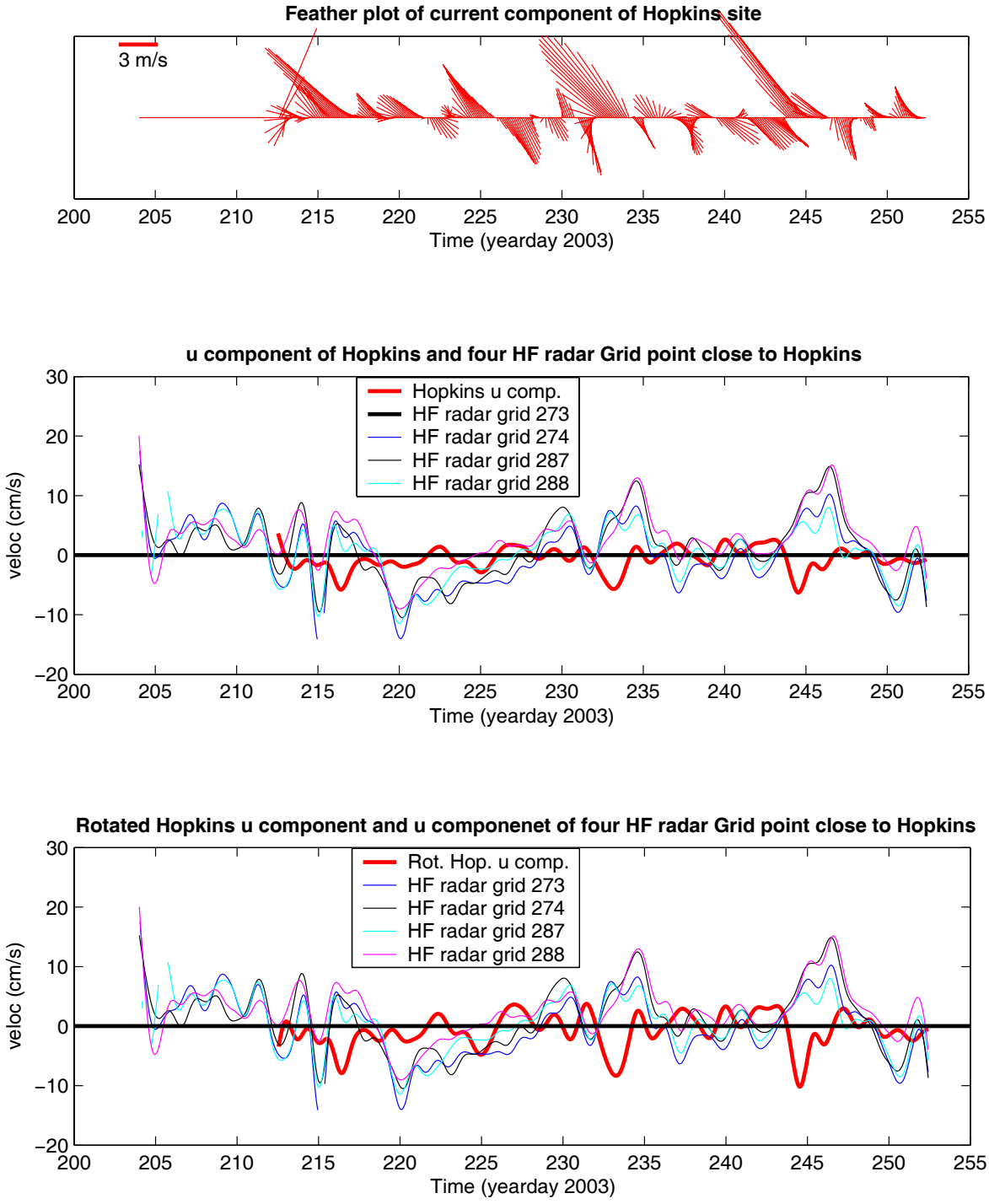

Figure 42. First plot depicts intensity and direction or surface current of Hopkins point. Second one, shows the comparison of non rotated u component of Hopkins and closest HF radar grid points and the third plot shows rotated u component and same HF radar grid points.

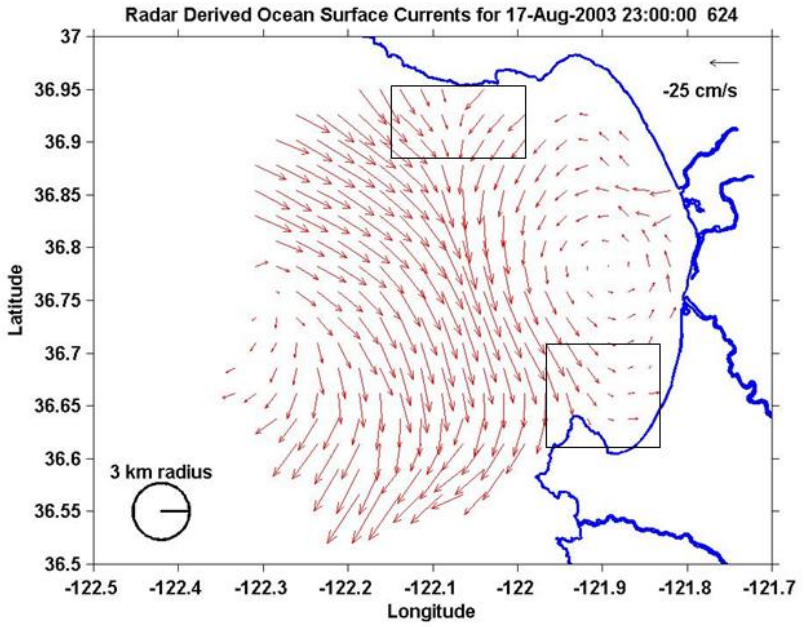

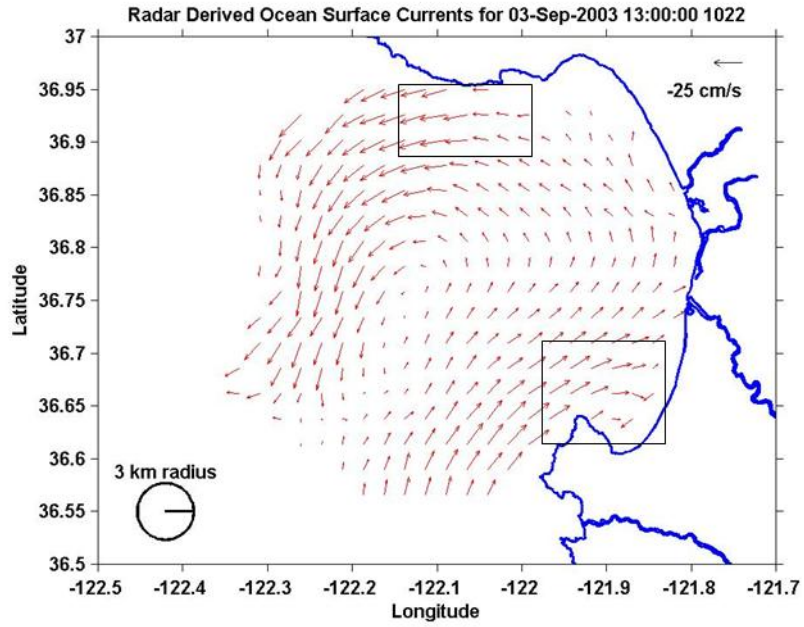

Figure 43. Surface Current map indicating the sense of the flow in Hopkins and Terrace site.

IV. DISCUSSION AND RESULTS

A. WINDS EFFECTS

Winds in Monterey Bay often fluctuate between persistent periods of upwelling favorable conditions and brief periods of relaxation with a shift in the wind direction. In this study, coastal wind fields were observed from June, 2003 to March, 2004. Northerly winds predominated in summer to mid-fall with a reversal in the typical wind direction in late fall and winter. The periods of persistent upwelling favorable winds, wind blowing toward the southeast, occurred primarily during summer from late June to late October. These upwelling periods often lasted between five to ten days, even longer on some occasions, with speeds of about four to five m/s. These periods were interrupted by brief relaxations of the winds lasting just one to three days, sometimes less, and with winds shifting to the northeast or northwest with weaker intensity. During the upwelling periods, the typical circulation in the Bay consisted of a cyclonic circulation on shore sometimes accompanied with an anticyclonic circulation in the offshore area. When the wind stress was sustained for a longer period, the cyclonic circulation was more fully developed. The strongest currents were observed in the southern part of the bay, off Point Piños.

Downwelling events were more infrequent than the upwelling. These events start in late November until late February with duration between two to five days. The wind direction was often toward the northwest, with stronger intensity than the upwelling periods but for shorter times. In these periods, the wind stress relaxes and cooler upwelled water starts to sink and become replaced by warmer waters.

Other wind directions were also analyzed. These however are much less common. Wind blows from the northeast and from the southwest, often during late summer and fall with short duration and low intensity but with important influences on the surface current patterns.

B. OCEAN CURRENT PATTERN RECOGNITION

Surface current patterns around Monterey Bay have strong variability that is well separated in terms of its temporal and spatial scales. During upwelling and downwelling conditions the surface current generally aligns with the wind in the offshore areas. The flow responds almost immediately (i.e., within hours) to the wind stress. This result is, at least, partially related to the fact that the HF radar systems calculate the speed of the skin of the water, probably less than one meter in depth, so the observed response of the surface current to the wind stress happens very quickly. In shore areas within the 1-3 km resolution of the HF radar network, the current responses are uncertain. The current meter records analyzed in this study from the PISCO project were deployed only a few hundred meters from the shore in 15-20 m water depths. Because of the closeness to the coastline, those currents were observed to flow predominantly alongshore.

During upwelling conditions, the wind speed and direction time series exhibit long duration events, which tend to spin up counterclockwise circulations in the middle of the bay. This circulation becomes stronger when the period of the event is longer. For a specific condition of the wind direction, this is when it blows from the north (320^0 to 050^0), the surface current is very sensitive to a small change in the direction between or close to that angle-wedge without changing the wind intensity. This sensitivity refers to the intensity of gyres that are formed in the bay.

During downwelling, the current patterns align very well off shore and tend to align with the coastline inshore. The surface current is stronger out of the bay reaching a speed of about 25 to 30 cm/s and slowing down when entering the bay. When the wind blows from the southwest, the current flows into the bay in the northern area and then veers to the left, aligning with the coastline. A weak counterclockwise circulation forms into the bay and a second one out of the bay. When the wind shifts and blows from the northeast, the current flows into the bay off Point Piños and then turns to the left, following the coastline.

When the wind blows from the northeast, for a period up to 24 hours, a clockwise circulation forms in the middle of the bay and a strong current flushes out of the bay off Point Piños. When southwest winds occur, often during summer and fall for a brief period and with weak intensity, a well developed anticyclonic gyre forms in the middle of the bay, flushing out a strong current in the northern areas with intensities of about 30 cm/s.

The two areas close to the shore that were also analyzed, Hopkins and Terrace point, must be investigated with special care due to their proximity to the coastline. The alongshore flow at the Hopkins site has negative sign indicating flow moving out of the bay during most of the analysis period, which corresponds to upwelling favorable wind conditions. But further north, on the HF radar grid points close to the Hopkins site, the flows had positive sign—goes into the Bay. According to this, it can be inferred that when the wind blows from the north-northwest during upwelling favorable wind conditions, a small clockwise gyre forms in that area, probably due to the geographic characteristics of that area.

At Terrace Point, the area where the bottom-fixed ADCP was located is an area where the surface currents tend to converge during upwelling favorable winds as can be seen in Figure 43. Generally, where the ADCP was located the flow moved out of the bay during the time of the analysis. Further south, where the line of six HF grid points were selected and the flow had both positive and negative sign, the flow moved into the Bay in the western area and out of the bay in the eastern area.

THIS PAGE INTENTIONALLY LEFT BLANK

V. CONCLUSIONS

This study investigated the patterns of surface ocean currents in Monterey Bay over a period of ten months during which continuous, hourly observations were available from a 5-site HF radar network. Continuous observations of offshore winds were also available from the M1 mooring maintained by MBARI. These records made it possible to describe the common current patterns under a variety of wind conditions. In all cases, both the surface current and near-surface wind data were low-pass-filtered to remove diurnal-period fluctuations, which means that the patterns investigated in this study are related to the low-frequency variations in the wind forcing. The most important of these variations is the cycling between upwelling favorable alongshore winds and shorter periods of relaxed or downwelling favorable winds. This cycling is dominant from spring through fall. Only in the winter period do strong synoptic events, which can have wind directions other than alongshore, dominate in this region.

In areas close to the shore, such as the Hopkins and Terrace Point locations studied here in the southern and northern portions of Monterey Bay, respectively, the currents are confined to flow alongshore. It is possible to relate the near-coastal currents to the larger surface current patterns, although the relationships would not be obvious from the near-coastal records alone. In the southern example, the offshore flow tends to be opposite to the near-coastal flow due to a small circulation cell that appears to form in the southeastern portion of Monterey Bay. Along the northern coastline near Terrace Point, the flow is correlated with the offshore flow observed by the HF radar network but the correlation is degraded because the flow offshore of that site is often observed to be convergent in terms of the east-west (or cross shore) flow direction.

The MATLAB-based HFRadarmap toolbox was an excellent tool for computing and mapping the surface current in the Monterey Bay over the long term and in real time. The toolbox extension developed in this project, namely the program used to perform conditional averaging of the surface currents based on

specified conditions on the observed wind speeds, directions, and durations, was very informative. Given the long records, it was possible to create significant average surface current maps that were based on ensemble realizations over several different events. This was particularly true for the dominant upwelling favorable wind conditions for which it was shown that cyclonic circulation inside Monterey Bay forms within a day of the onset of upwelling winds. Furthermore, if those winds persist for more than a day, it was shown that the circulation pattern becomes more intense and well defined. In the converse situation during the shorter-duration downwelling winds, the surface currents were seen to respond quickly to the new forcing and to set up reversed, northward-flowing currents, particularly in the region across the mouth of Monterey Bay.

Finally, less well represented wind conditions, such as winds blowing toward the southwest, were shown to produce interesting surface current patterns. These include rare but potentially important “flushing events” for which strong currents move water out of the bay along the southern shoreline. Even for the more common conditions in which winds were observed to blow toward the south, the conditional averaging employed in this study showed that the surface current patterns that develop can be very sensitive to wind direction. A change of just 5-10 degrees in wind direction was shown to be enough to produce a well-developed, two-gyre system in one case and not in the other.

It is recommended that the conditional averaging approach used in this study be extended to longer time series and, possibly, to other test records, such as winds from additional mooring sites or the near-coastal currents provided by the PISCO project. It is through the combined use of single-point indices and the two-dimensional maps from HF radar that the maximum benefit of the unique HF radar data can be realized.

LIST OF REFERENCES

Breaker, L. C., and W. W. Broenkow, 1994: *The Circulation of Monterey and related processes*. Oceanography and Marine Biology: an Annual Review, 32. 1-64.

Chavez, F. P., Herlien, R. and Thurmond, G., 1997: *Real time experimental moorings: An OASIS in Monterey Bay, California.* Web Site: *http*://*www.mbari.org/bog/Projects/MOOS/oasis/oasis*.

Cook, M. S., Paduan, J. D., 1999: *Processing HF radar Data using the HFRadarmap Software System.* Technical Report, 15 pp.

Codar Ocean Sensors, Ltd. Web site: *http://www.codaros.com.*

Drake, P., UCSC PISCO, 1999: *Subtidal Physical Oceanography File Naming Convention and Data Processing, UCSC Technical Report, 14 pp.*

Emery, W. J. and R.E. Thomson, 2001: *Data Analysis Methods in Physical Oceanography.* Second and Revised Edition, Elsevier Press, Amsterdam, 638 pp.

Ferziger, J.H., and Tseng Y.H., 2003: Numerical *Simulation of Regional Circulation in the Monterey Bay Region. Web Site; http://ctr.stanford.edu/ResBriefs03/yhtseng.pdf.*

Hickey, B. M., 1998: *Coastal Oceanography of* w*estern North America, from the tip of Baja California to Vancouver Island.* In: The Sea, Vol 11, Willey, J., New York, 1062 pp.

Lynn, R. J., and J. J. Simpson, 1987: *The California Current System: The Seasonal Variability of its Physical Characteristics*. J. Geophys. Res., 92, 12947-12966.

MBARI-BOG, 1999: *A ten-year time series from Monterey Bay, California: Seasonal, interannual and long-term patterns. Web site:* http://www.mbari.org/bog/Projects.

Paduan, J. D., and L. K. Rosenfeld, 1996: *Remotely sensed surface currents in Monterey Bay from shore-based HF radar (Coastal Ocean Dynamics Application Radar).* J. Geophys. Res., 101, 20669-20686.

Pickard, G.L., and W. J. Emery, 1964*: Descriptive Physical Oceanography*. Fifth Edition, Pergamon, Press, Oxford, 320 pp.

Ramp, S. R, L. K. Rosenfeld, T. D. Tisch, and M.R. Hicks, 1997: *Moored observations of the current and temperature structure over the continental slope off California: A basic description of the variability*. J. Geophys. Res.,102, 22877-22902.

Rosenfeld, L. K. F. B. Schwing, N. Garfield, and D. E. Tracy, 1994: *Bifurcated flow from an upwelling center: a cold water source for Monterey Bay*. Continental Shelf Res., 14 No. 9. 931-964.

Smith, Jr., Albert A., 1998*: Radio Frequency Principles and Applications*. IEEE Press, New York, 219 pp.

Skogsberg, T., 1936: *Hydrography of Monterey Bay, California. Thermal conditions, 1929-1933.* Transactions of the American Philosophical Society, 29. 1-152.

Strub, P. T., J. S. Allen, A. Huyer, and R. L. Smith, 1987: *Seasonal Cycles of Currents, Temperatures, Winds and Sea Level over the Northeast Pacific Continental Shelf: 35^0 N to 48^0 N.,* J. Geophy. Res., 92.1507-1526.

Tomczak, M., and J. Stuart Godfrey, 2003: *Regional Oceanography*: *An Introduction.* Pergamon Press, Oxford, 422 pp.

INITIAL DISTRIBUTION LIST

1. Dudley Knox Library
   Naval Postgraduate School
   Monterey, CA

2. Dr. Jeffrey Paduan
   Department of Oceanography
   Naval Postgraduate School
   Monterey, CA

3. Dr. Mary Batteen
   Department of Oceanography
   Naval Postgraduate School
   Monterey, CA

4. Dr. Curtis Collins
   Department of Oceanography
   Naval Postgraduate School
   Monterey, CA

5. Mr. Mike Cook
   Department of Oceanography
   Naval Postgraduate School
   Monterey, CA

6. Mr. Fred Bahr
   Department of Oceanography
   Naval Postgraduate School
   Monterey, CA

7. Dr. Leslie Rosenfeld
   Department of Oceanography
   Naval Postgraduate School
   Monterey, CA